Aerosol effects on liquid-water path of thin stratocumulus clouds

Seoung Soo Lee,[1] Joyce E. Penner,[1] and Stephen M. Saleeby[2]

Received 29 May 2008; revised 5 December 2008; accepted 2 February 2009; published 3 April 2009.

[1] Thin clouds with mean liquid water path (LWP) of $\sim$50 g m^{-2} cover 27.5% of the globe and thus play an important role in Earth's radiation budget. Radiative fluxes at Earth's surface and top of atmosphere are very sensitive to the LWP variation when the LWP becomes smaller than $\sim$50 g m^{-2}. This indicates that aerosol effects on thin clouds can have a substantial impact on the variation of global radiative forcing if LWP changes. This study examines the aerosol indirect effect through changes in the LWP in three cases of thin warm stratocumulus clouds with LWP < 50 g m^{-2}. We use a cloud-system resolving model coupled with a double-moment representation of cloud microphysics. Intensified interactions among the cloud droplet number concentration, condensation, and dynamics at high aerosol play a critical role in the LWP responses to aerosol increases. Increased aerosols lead to increased CDNC, providing the increased surface area of droplets where water vapor condenses. This increases condensation, and thus condensational heating, to produce stronger updrafts, leading to an increased LWP with increased aerosols in two of the cases where precipitation reaches the surface. In a case with no surface precipitation, LWP decreases with increases in aerosols. In this case, most of precipitation evaporates just below the cloud base. With decreases in aerosols, precipitation increases and leads to increasing evaporation of precipitation, thereby increasing instability around the cloud base. This leads to increased updrafts, and thus condensation, from which increased LWP results.

Citation: Lee, S. S., J. E. Penner, and S. M. Saleeby (2009), Aerosol effects on liquid-water path of thin stratocumulus clouds, *J. Geophys. Res.*, *114*, D07204, doi:10.1029/2008JD010513.

1. Introduction

[2] Aerosol concentrations have increased significantly as a result of industrialization. Increasing aerosols are generally considered to offset global warming by reflecting incoming solar radiation. Increasing aerosols are known to decrease droplet size and thus increase cloud albedo (first AIE) [*Twomey*, 1974, 1977]. They may also suppress precipitation and, hence, alter cloud mass and lifetime (second AIE) [*Albrecht*, 1989]. The AIE is uncertain, since AIE accompanies cloud microphysics; uncertainties of radiative forcing associated with AIE are comparable to radiative forcing by an anthropogenic increase in green house gases [*Ramaswamy et al.*, 2001; *Forster et al.*, 2007].

[3] *Turner et al.* [2007] showed that low-level stratiform clouds with mean LWP of only 51 g m^{-2} cover 27.5% of the globe. Other studies have also shown that thin clouds accounted for a significant portion of cloudiness at continental midlatitude sites and in the Arctic and tropical regions [*McFarlane and Evans*, 2004; *Shupe and Intrieri*, 2004; *Marchand et al.*, 2003]. Hence, *Turner et al.* [2007] postulated that these thin clouds were undeniably important to many aspects of atmospheric sciences and intertwined with the broader climate. *Turner et al.* [2007] showed that surface and TOA longwave and shortwave radiative fluxes are very sensitive to small changes in the cloud LWP when the LWP is less than $\sim$50 g m^{-2} [*Turner et al.*, 2007, Figure SB1]. This strong sensitivity was simulated in both summer and winter atmospheres for representative particle sizes of both continental and maritime clouds. This indicates that the strong sensitivity of the fluxes at low LWP was fairly robust to environmental conditions and to the size of particles. Aerosols are known to change cloud properties including LWP [*Albrecht*, 1989; *Ackerman et al.*, 2004; *Guo et al.*, 2007]. Hence, above mentioned studies suggest that global radiation budgets can be more susceptible to aerosol-induced changes in LWP in thin clouds than comparatively thick clouds. This demonstrates that the assessment of aerosol effects on thin clouds can be critical for a better assessment of aerosol effects on clouds and thus climate.

[4] This study aims to gain a preliminary understanding of aerosol–cloud interactions in thin stratiform clouds. Three cases of thin warm stratocumulus clouds with LWP < 50 g m^{-2} are simulated to achieve the goal of this study. These clouds develop under different humidity conditions around the top of the planetary boundary layer (PBL): wet, moderately wet and dry conditions. Average humidity around the top of the PBL in the wet, moderately wet and dry conditions is $\sim$80%, 60%, and 40%, respectively. These simulations are forced using the reanalysis data

[1]Department of Atmospheric, Oceanic, and Space Sciences, University of Michigan, Ann Arbor, Michigan, USA.
[2]Department of Atmospheric Science, Colorado State University, Fort Collins, Colorado, USA.

0148-0227/09/2008JD010513

from European Centre for Medium-Range Weather Forecast (ECMWF) in summer 2002 over the North Atlantic where significant increases in aerosols have been observed since industrialization.

[5] Two experiments are conducted for each humidity condition using the Goddard Cumulus Ensemble (GCE) model coupled to a double-moment microphysics scheme. The first and second experiments use present-day and preindustrial aerosol profiles from the NCAR Community Atmospheric Model (CAM3) coupled with Integrated Massively Parallel Atmospheric Chemical Transport (IMPACT) atmospheric chemistry and aerosol transport model and, henceforth, are referred to as the "high-aerosol run" and "low-aerosol run," respectively. The comparison of the high- and low-aerosol runs identifies how a transition from clean preindustrial aerosols to polluted present-day aerosols affects clouds under constant large-scale forcing. This transition can also be translated as changes from maritime aerosols to clean continental aerosols. This is because preindustrial and present-day aerosols used in this study correspond to typical maritime and clean continental aerosols, respectively, according to the classification of *Whitby* [1978] (see section 4 for details).

[6] The double-moment microphysics predicts hydrometeor number as well as hydrometeor mass and the aerosol number and size distribution are considered for nucleation process. Most of bulk microphysics adopted empirical autoconversion parameterizations relying on threshold cloud-liquid mixing ratios. These empirical autoconversion parameterizations are based on the partition of the drop spectrum between cloud droplets and rain, which does not exist in reality. This causes uncertainties in the simulation of the conversion of small droplets to large droplets and raindrops, an important process associated with aerosol effects on the LWP and precipitation. To simulate the conversion process with better fidelity, a double-moment microphysics scheme used here employs full stochastic collection solutions with realistic collection kernels for self-collection among cloud droplets and the raindrop collection of cloud droplets. Also, the sedimentation of droplets and rain, which plays an important role in the LWP variation as reported in the work *Ackerman et al.* [2004], is simulated by emulating a full-bin model with 36 bins (see section 2.2 for details). This simulates the sedimentation with better confidence than previously treatments of sedimentation that use a mass-weighted fall speed.

2. CSRM

2.1. Dynamics and Turbulence

[7] For numerical experiments, the GCE model [*Tao et al.*, 2003] is used as a two-dimensional nonhydrostatic compressible model. The detailed equations of the dynamical core of the GCE model are described by *Tao and Simpson* [1993] and *Simpson and Tao* [1993].

[8] The subgrid-scale turbulence used in the GCE model is based on work by *Klemp and Wilhelmson* [1978] and *Soong and Ogura* [1980]. In their approach, one prognostic equation is solved for the subgrid-scale kinetic energy, which is then used to specify the eddy coefficients. The effect of condensation on the generation of subgrid-scale kinetic energy is also incorporated into the model.

2.2. Microphysics and Radiation

[9] To represent microphysical processes, the GCE model adopts the double-moment bulk representation of *Saleeby and Cotton* [2004]. The size distribution of hydrometeors obeys a generalized gamma distribution:

$$n(D) = \frac{N_t}{\Gamma(\upsilon)} \left(\frac{D}{D_n}\right)^{\nu-1} \frac{1}{D_n} \exp\left(-\frac{D}{D_n}\right) \quad (1)$$

where D is the equivalent spherical diameter (m), $n(D)dD$ the number concentration (m^{-3}) of particles in the size range dD and N_t the total number of particles (m^{-3}). Also, ν is the gamma distribution shape parameter (nondimensional) and D_n is the characteristic diameter of the distribution (m).

[10] Full stochastic collection solutions for self-collection among cloud droplets and for raindrop collection of cloud droplets based on *Feingold et al.* [1988] are obtained using realistic collection kernels from *Long* [1974] and *Hall* [1980]. Hence, this study does not constrain the system to constant or average collection efficiencies. Following *Walko et al.* [1995], lookup tables are generated and used in each collection process. This enables fast and accurate solutions to the collection equations.

[11] The philosophy of bin representation of collection is adopted for calculations of drop sedimentation. Bin sedimentation is simulated by dividing the gamma distribution into discrete bins and then building lookup tables to calculate how much mass and number in a given grid cell falls into each cell beneath a given level in a given time step. Thirty-six bins are used for collection and sedimentation. This is because *Feingold et al.* [1999] reported that the closest agreement between a full bin-resolving microphysics model in a large eddy simulation (LES) of marine stratocumulus cloud and the bulk microphysics representation was obtained when collection and sedimentation were simulated by emulating a full-bin model with 36 bins.

[12] Cloud droplets are divided into small and large cloud droplets. Small and large cloud droplets range $2-40$ μm and $40-80$ μm in diameter, respectively. The 40-μm division between the two droplet modes is natural because it is well known that collection rates for droplets smaller than this size are very small, whereas droplets greater than this size participate in vigorous collision and coalescence. The large-cloud-droplet mode is allowed to interact with all other species (i.e., the small-cloud-droplet mode and rain for warm microphysics). The large-cloud-droplet mode plays a significant role in the collision-coalescence process by requiring droplets to grow at a slower rate as they pass from the small-cloud-droplet mode to rain, rather than being transferred directly from the small-cloud-droplet mode to rain.

[13] All the cloud species here have their own terminal velocity. The terminal velocity of each species is expressed as power law relations [see *Walko et al.*, 1995, equation (7)] on the basis of the fall-speed formulations in the work of *Rogers and Yau* [1989]. A Lagrangian scheme is used to transport the mixing ratio and number concentration of each species from any given grid cell to a lower height in the vertical column, following *Walko et al.* [1995].

[14] A Lagrangian parcel model [*Heymsfield and Sabin*, 1989; *Feingold and Heymsfield*, 1992] is used to construct lookup tables for use in droplet nucleation routine that predicts the percent of cloud condensation nuclei (CCN) that activate. The parcel model follows the Köhler equations and the cloud droplet growth formulation from *Pruppacher and Klett* [1997]. The parcel model represents the aerosol spectrum as a binned lognormal distribution, on the basis of the given number concentration and mode radius of CCN,

$$N(r) = \frac{N_{ccn}}{r\sqrt{2\pi}\ln\sigma}\exp\left\{\frac{-\left[\ln\left(r/r_g\right)\right]^2}{2\left(\ln\sigma\right)^2}\right\} \quad (2)$$

Here, r is the aerosol radius, N(r)dr is the number concentration of CCN in the size range dr, N_{ccn} is the total number concentration of CCN, σ is the standard deviation of the distribution, and r_g is the distribution mode radius. This distribution breaks up the total CCN number concentration into 200 mass bins ranging from 10^{-17} to 10^{-8} g with a distribution breath of $\sigma = 2.0$, a typical value for maritime aerosols [*Whitby*, 1978]. The CCN composition is assumed to consist of ammonium sulfate. The detailed description of the parcel model and the construction of lookup tables can be found in the work of *Saleeby and Cotton* [2004].

[15] The parameterizations developed by *Chou and Suarez* [1999] for shortwave radiation and by *Chou et al.* [1995], *Chou and Kouvaris* [1991], and *Kratz et al.* [1998] for longwave radiation have been implemented in the GCE model. The solar radiation scheme includes absorption owing to water vapor, CO_2, O_3, and O_2. Interactions among the gaseous absorption and scattering by clouds, molecules, and the surface are fully taken into account. Reflection and transmission of a cloud layer are computed using the δ-Eddington approximation. Fluxes for a composite of layers are then computed using the two-stream adding approximation. In computing thermal infrared fluxes, the k-distribution method with temperature and pressure scaling is used to compute the transmission function.

3. Case Descriptions

[16] Three cases of thin marine stratocumulus are simulated here. They are under different humidity conditions near the top of the PBL. The first, second, are third cases are located at (42°N, 63°W), (46°N, 60°W), and (42°N, 53°W), respectively. The average relative humidity at the top of the PBL over the simulation period is ~80%, 60%, and 40% in the first, second, and third cases, respectively. Henceforth, the first, second, and the third cases are referred to as "WET," "MID-WET" and "DRY," respectively. Vertical profiles of initial specific humidity, potential temperature and horizontal wind velocity are shown in Figure 1 for those three cases. The wind is eastward in WET and DRY, whereas it is westward in MID-WET. For each case, a pair of 12-hour simulations from 0200 to 1400 LST (local solar time) are performed in which the aerosol concentration is varied from the preindustrial level for the low-aerosol run to the present-day level for the high-aerosol run.

[17] The reanalysis data from ECMWF provide large-scale forcing. The 6-hourly analyses were applied to the model as the large-scale advection for potential temperature and specific humidity at every time step by interpolation. Temperature and humidity were nudged toward the large-scale fields from ECMWF with a relaxation time of one hour using the large-scale advection. The horizontally averaged wind from the GCE model was also nudged toward the interpolated wind field from ECMWF at every time step with a relaxation time of one hour, following *Xu et al.* [2002]. The model domain is considered to be small compared to large-scale disturbances. Hence, the large-scale advection is approximated to be uniform over the model domain and large-scale terms are defined to be functions of height and time only, following *Krueger et al.* [1999]. Identical observed surface fluxes of heat and moisture were prescribed in both the high- and low-aerosol runs. This method of modeling cloud systems was used for the CSRM comparison study by *Xu et al.* [2002]. The details of the procedure for applying large-scale forcing are described in the work of *Donner et al.* [1999] and are similar to the method proposed by *Grabowski et al.* [1996].

[18] Time- and domain-averaged large-scale advective temperature (humidity) tendency is ~2.0 K d^{-1} (2.5 g kg^{-1} d^{-1}) in WET and WET is forced by positive temperature and humidity advection throughout the PBL. MID-WET and DRY are also forced by positive temperature and humidity advection throughout the PBL. Time- and domain-averaged temperature (humidity) tendency is ~2.0 K d^{-1} (3.0 g kg^{-1} d^{-1}) in MID-WET. In DRY, the averaged temperature (humidity) forcing is ~2.0 K d^{-1} (3.5 g kg^{-1} d^{-1}). Time-averaged large-scale subsidence is ~0.30, 0.71, and 0.22 cm s^{-1} in WET, MID-WET, and DRY, respectively, around top of the PBL.

4. Integration Design and Aerosol Specification

[19] All of the simulations are performed in a 2-D framework. The horizontal domain uses 508 grid points with a uniform grid length of 50 m. The vertical grid length is uniformly 40 m below 2 km and then stretches to 240 m near the model top. The vertical domain is 20 km and the time step is 0.5 s. Periodic boundary conditions are set on horizontal boundaries and a damping layer of 5 km depth is applied near the model top.

[20] The profiles of total aerosol number for present-day and preindustrial conditions are calculated from predicted aerosol mass in the CAM3 [*Collins et al.*, 2006a, 2006b] coupled with the IMPACT model [*Rotman et al.*, 2004; *Penner et al.*, 1998]. In this coupled model system, meteorological fields generated from the coupled CAM3 model are available at each time step of the IMPACT model. The IMPACT model used here is an extended version of that described in the work of *Liu and Penner* [2002] to treat the mass of sulfate aerosol as a prognostic variable, and is further extended in the work of *Liu et al.* [2005] to treat the microphysics of sulfate aerosol using a modal representation [*Herzog et al.*, 2004]. The IMPACT model simulates the dynamics of sulfate aerosol (nucleation, condensation, and coagulation) and its interactions with primary emitted non-sulfate aerosols: organic matter (OM), black carbon (BC), dust and sea salt, using a modal representation of aerosol microphysics with an arbitrary number of modes [*Herzog et al.*, 2004; *Liu et al.*, 2005]. The predicted monthly mean

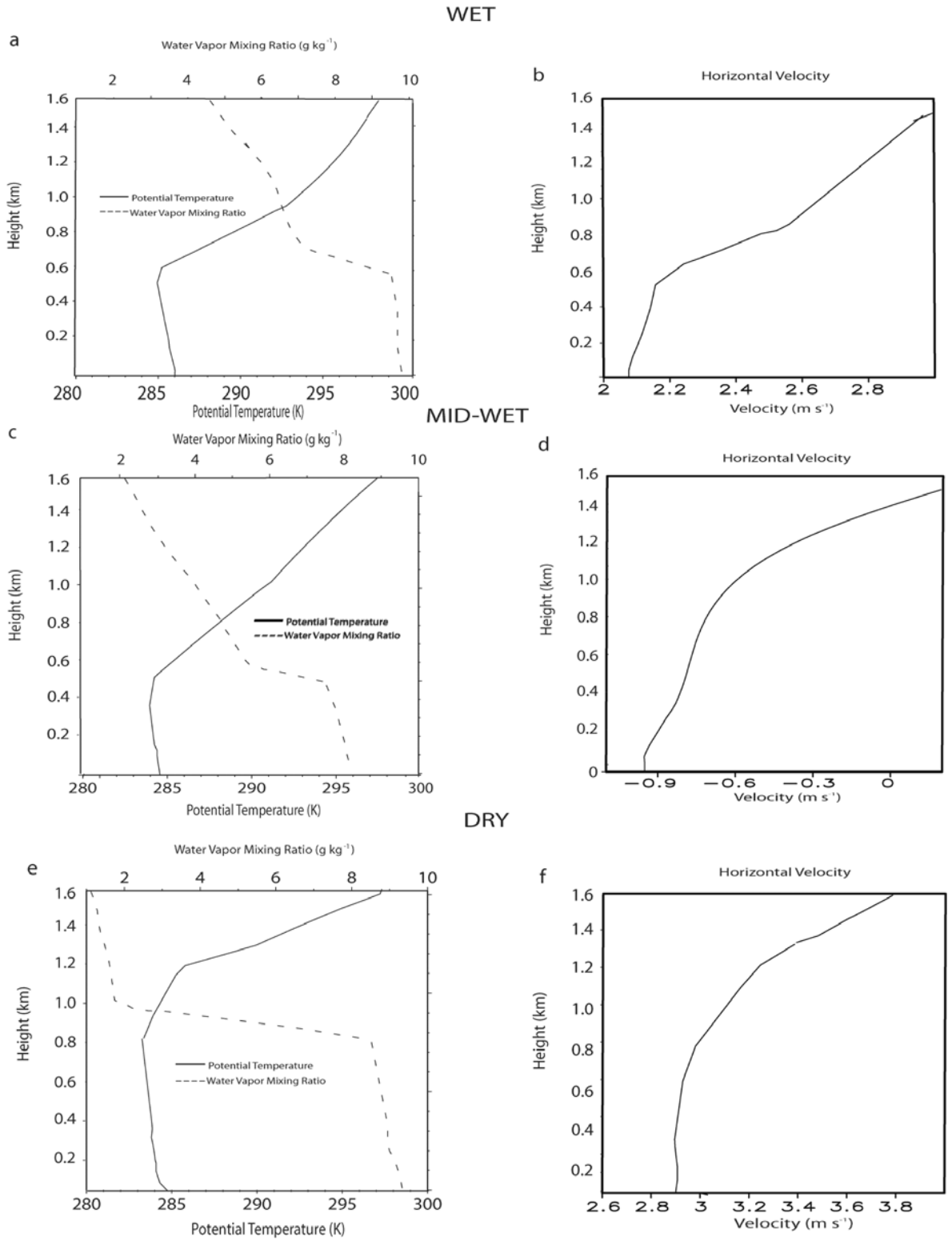

Figure 1. Vertical profiles of initial potential temperature, water vapor mixing ratio, and initial horizontal wind velocity for (a and b) WET, (c and d) MID-WET, and (e and f) DRY.

mass profiles of aerosols are obtained at (42°N, 63°W), (46°N, 60°W) and (42°N, 53°W) for WET, MID-WET, and DRY, respectively, in June. Anthropogenic aerosol emissions from *Smith et al.* [2001, 2004] and *Ito and Penner* [2005] for the years 2000 and 1850 are used for the calculation of aerosol profiles. Aerosol profiles from years 2000 and 1850 represent present-day and preindustrial profiles, respectively. Natural emissions are prescribed to

Table 1. Summary of Simulations With the Different Aerosols and Application of CDNC to Model Processes

Simulations	Background Aerosols Averaged Over the PBL (cm^{-3})	CDNC
	WET	
High-aerosol run	3100	predicted for all processes
Low-aerosol run	1200	predicted for all processes
High-aerosol run (CDNC-high fixed)	3100	fixed at 242 cm^{-3} (for condensation)/predicted (for the other processes)
Low-aerosol run (CDNC-high fixed)	1200	fixed at 242 cm^{-3} (for condensation)/predicted (for the other processes)
High-aerosol run (CDNC-low fixed)	3100	fixed at 39 cm^{-3} (for condensation)/predicted (for the other processes)
Low-aerosol run (CDNC-low fixed)	1200	fixed at 39 cm^{-3} (for condensation)/predicted (for the other processes)
	MID-WET	
High-aerosol run	3200	predicted for all processes
Low-aerosol run	1100	predicted for all processes
High-aerosol run (CDNC-high fixed)	3200	fixed at 202 cm^{-3} (for condensation)/predicted (for the other processes)
Low-aerosol run (CDNC-high fixed)	1100	fixed at 202 cm^{-3} (for condensation)/predicted (for the other processes)
High-aerosol run (CDNC-low fixed)	3200	fixed at 40 cm^{-3} (for condensation)/predicted (for the other processes)
Low-aerosol run (CDNC-low fixed)	1100	fixed at 40 cm^{-3} (for condensation)/predicted (for the other processes)
	DRY	
High-aerosol run	2200	predicted for all processes
Low-aerosol run	1100	predicted for all processes
High-aerosol run $\times$ 2	4400	predicted for all processes
Low-aerosol run/10	110	predicted for all processes

be the same for the calculation of present-day and preindustrial aerosols. A more detailed description of the coupled system and the calculation of aerosol profiles can be found in the work by *Wang and Penner* [2009].

[21] Aerosol number concentration is calculated from the mass profiles using parameters (mode radius, standard deviation, and partitioning of among modes) of multimodal aerosol size distributions described in the work of *Liu et al.* [2005]. The calculated aerosol number only in the accumulation mode acts as background aerosols and is adopted by the droplet nucleation scheme here. This is because the parcel model assumes a unimodal lognormal size distribution of aerosols (see equation (2)) and, generally, most CCN are in the accumulation mode of the distribution for the low supersaturations ($\sim$0.05%) generally observed in stratiform clouds. All aerosols are assumed to consist of ammonium sulfate as assumed in the droplet nucleation scheme here. Hence, this study does not take into account the effects of aerosol chemical composition and only focuses on effects of aerosol number on clouds. This is consistent with the findings of *Saleeby and Cotton* [2004] which noted that the chemical composition of aerosols led to a much smaller variability in the fraction of activated aerosols as compared to aerosol number. In the PBL, the aerosol number is nearly constant and only varies vertically within 10% of its value at the surface. Vertically varying (and horizontally homogeneous in the model domain) present-day (preindustrial) background aerosol number, averaged over the PBL, is 3100 (1200), 3200 (1100), and 2200 (1100) cm^{-3} for the WET, MID-WET, and DRY, respectively. These numbers indicate that present-day and preindustrial aerosols correspond to typical clean continental and maritime aerosols, respectively [*Whitby*, 1978].

[22] The aerosol number concentration is predicted within cloud and reset to the background value at all levels outside cloud. Within clouds, aerosols are advected, diffused and depleted by nucleation (nucleation scavenging). The standard deviation of the assumed unimodel size distribution of aerosols is assumed not to vary spatiotemporally. The mode radius of the size distribution is predicted on the basis of the predicted aerosol number using *Saleeby and Cotton* [2004, equation (10)]. Initially, the aerosol number is everywhere set equal to its background value.

[23] Our focus is not on the effects of diurnal and daily variations of aerosols on clouds but on those of representative background present-day and preindustrial aerosols at the locations of simulations in June. In other words, our focus is on the examination of cloud responses to a representative aerosol variation since industrialization for the month of June. Hence, the diurnal and daily variations of aerosols owing to large-scale advection are not taken into account in this study. This is equivalent to assuming no advection of unactivated aerosols into and out of model domain, enabling us to assume that background aerosols do not vary spatiotemporally during time integration.

[24] Table 1 summarizes simulations in this study. In addition to the high- and low-aerosol runs, Table 1 shows that supplementary sensitivity tests are performed in WET and MID-WET. These tests are performed by changing the application of CDNC to model processes in WET and MID-WET (as briefly described in Table 1) and referred to as the high-aerosol run (CDNC-high fixed), low-aerosol run (CDNC-high fixed), high-aerosol run (CDNC-low fixed) and low-aerosol run (CDNC-low fixed). They will be described in more detail in section 5.4. In DRY, the additional tests are conducted by changing aerosols as briefly described in Table 1 and referred to as the high-

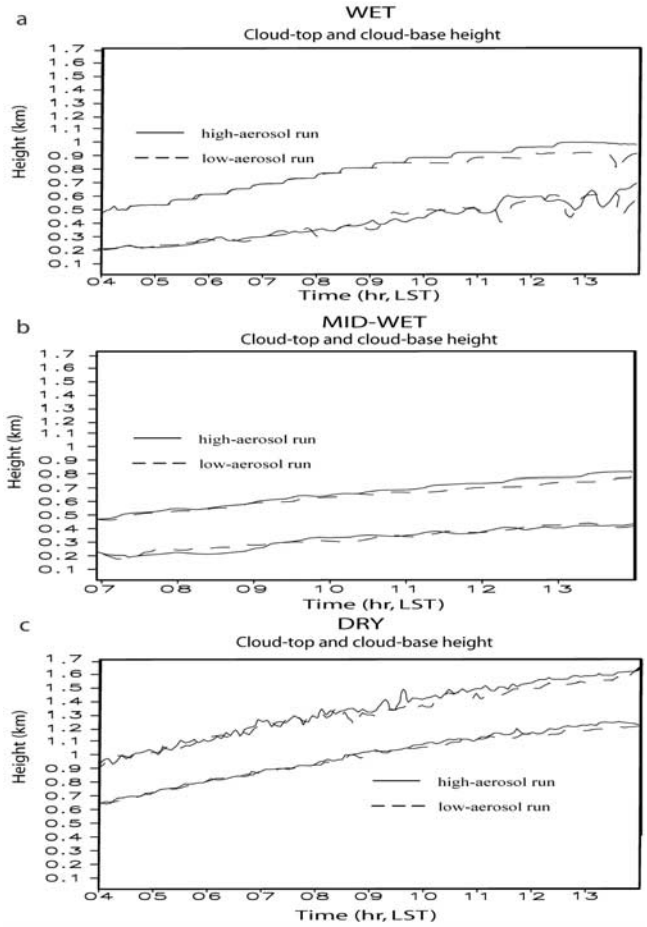

Figure 2. Time series of cloud top and cloud base height for (a) WET, (b) MID-WET, and (c) DRY. The upper (lower) two lines represent cloud top (cloud base) height.

aerosol run x 2 and the low-aerosol run/10. These tests will be discussed in more detail in section 5.6.

5. Results

5.1. Cloud Properties

[25] Clouds in WET and DRY are formed around 0300 LST and clouds in MID-WET are formed around 0600 LST. Figure 2 depicts the temporal evolution of cloud top and cloud base height (upper two lines are for cloud top and lower two lines for cloud base) and Figure 3 the evolution of cloud fraction for WET, MID-WET and DRY from ~1 hour after the cloud formation to the end of simulations. Figures 2 and 3 indicate maximum (minimum) cloud depth is ~400 (200) m and cloud fraction is always above 0.8 in WET. In MID-WET (DRY), cloud depth is between ~300 (200) and ~400 (400) and cloud fraction is always greater than 0.95 (0.95). These demonstrate that stratocumulus clouds in all three cases are shallow and maintain solid cloud decks with no substantial breakup.

[26] Averaged surface precipitation rates are 5.7×10^{-3} (1.5×10^{-2}) and 1.4×10^{-3} (3.6×10^{-3}) mm d^{-1} at high (low) aerosol for WET and MID-WET, respectively. In DRY, precipitation does not reach the surface.

[27] Average cloud top growth rates are higher (slightly lower) at high aerosol than at low aerosol in WET and MID-WET (DRY). Average growth rates are 1.15 (0.93), 0.78 (0.56) and 1.78 (1.80) cm s^{-1} at high (low) aerosol for WET, MID-WET and DRY, respectively (see Figure 2). The entrainment rate can be approximated by the difference between the cloud top growth rate and the large-scale vertical velocity [*Moeng et al.*, 1999; *Jiang et al.*, 2002; *Stevens et al.*, 2003a, 2003b]. The large-scale vertical velocity (subsidence) at high aerosol is the same as that at low aerosol around the top of clouds in each case. Hence, the entrainment rate is higher (slightly lower) in the high-aerosol run than in the low-aerosol run in WET and MID-WET (DRY). Larger large-scale subsidence around cloud top contributes to smaller cloud top growth rate in MID-WET than in WET and DRY. Also, larger large-scale subsidence around cloud top contributes to smaller cloud top growth rate in WET than in DRY.

[28] Figure 4 shows the temporal evolution of domain-averaged LWP for WET, MID-WET and DRY from ~1 hour after cloud formation to the end of simulations. LWPs are mostly below 50 g m^{-2} except for the high-aerosol run in WET where the LWP reaches its maximum value of ~60 g m^{-2} around 0800 LST. Figure 4 shows that the LWPs in the high-aerosol runs are generally higher than those in the low-aerosol runs in WET and MID-WET during time integration. Time- and domain-averaged LWPs are 46.15 (35.43) and 22.95 (18.54) g m^{-2} at high (low) aerosol in WET and

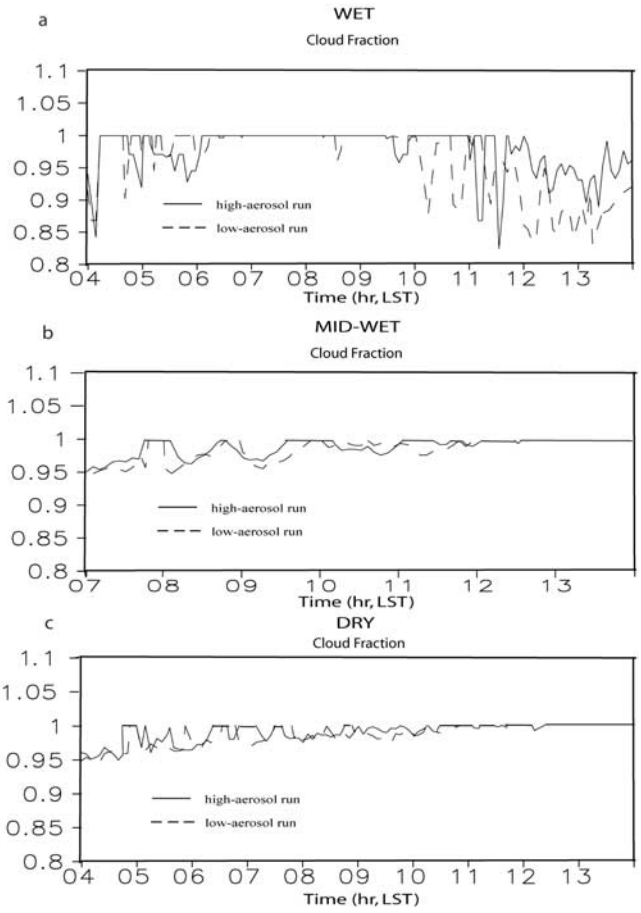

Figure 3. Time series of cloud fraction for (a) WET, (b) MID-WET, and (c) DRY.

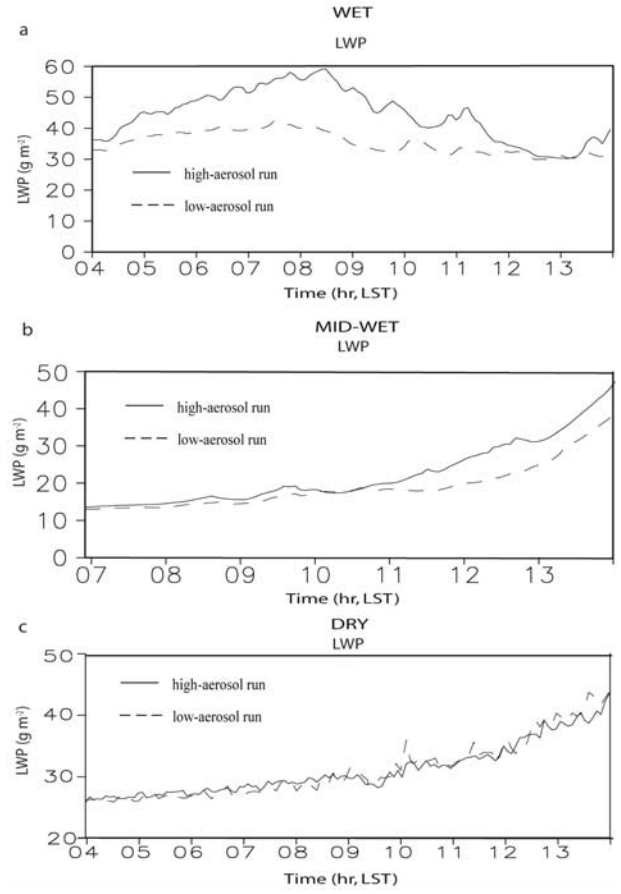

Figure 4. Time series of the domain-averaged LWP for (a) WET, (b) MID-WET, and (c) DRY.

MID-WET, respectively. However, the differences in LWP are much smaller in DRY than in WET and MID-WET. Time- and domain-averaged LWPs are 29.70 (30.21) g m^{-2} at high (low) aerosol in DRY; the time average of variables is performed over 0300–1400 LST for WET and DRY, and, in MID-WET, the time average is performed over 0600–1400 LST, unless otherwise stated. The low-aerosol run shows slightly higher LWP than the high-aerosol run in DRY. Since all averaged LWPs are <50 g m^{-2}, clouds here can be considered shallow according to the classification of *Turner et al.* [2007]. LWP begins to steadily increase ~4 h and 6 h after the cloud formation in MID-WET and DRY, respectively, owing to gradual increases in large-scale temperature and humidity tendency in the PBL. Figure 5 shows time- and domain-averaged vertical distribution of liquid water content (LWC). Consistent with the LWP responses to aerosols, LWCs are generally higher at high aerosol in WET and MID-WET and slightly lower at high aerosol in DRY. The vertical extent of LWC in Figure 5 is larger than maximum cloud depth shown in Figure 2 in each case. This is because cloud top and cloud base height generally increases with time.

[29] Simulated LWPs in the high-aerosol runs are compared to observations by the Moderate Resolution Imaging Spectroradiometer (MODIS) to assess the ability of the model to simulate stratiform clouds. The difference between the domain-averaged LWP in the high-aerosol run and

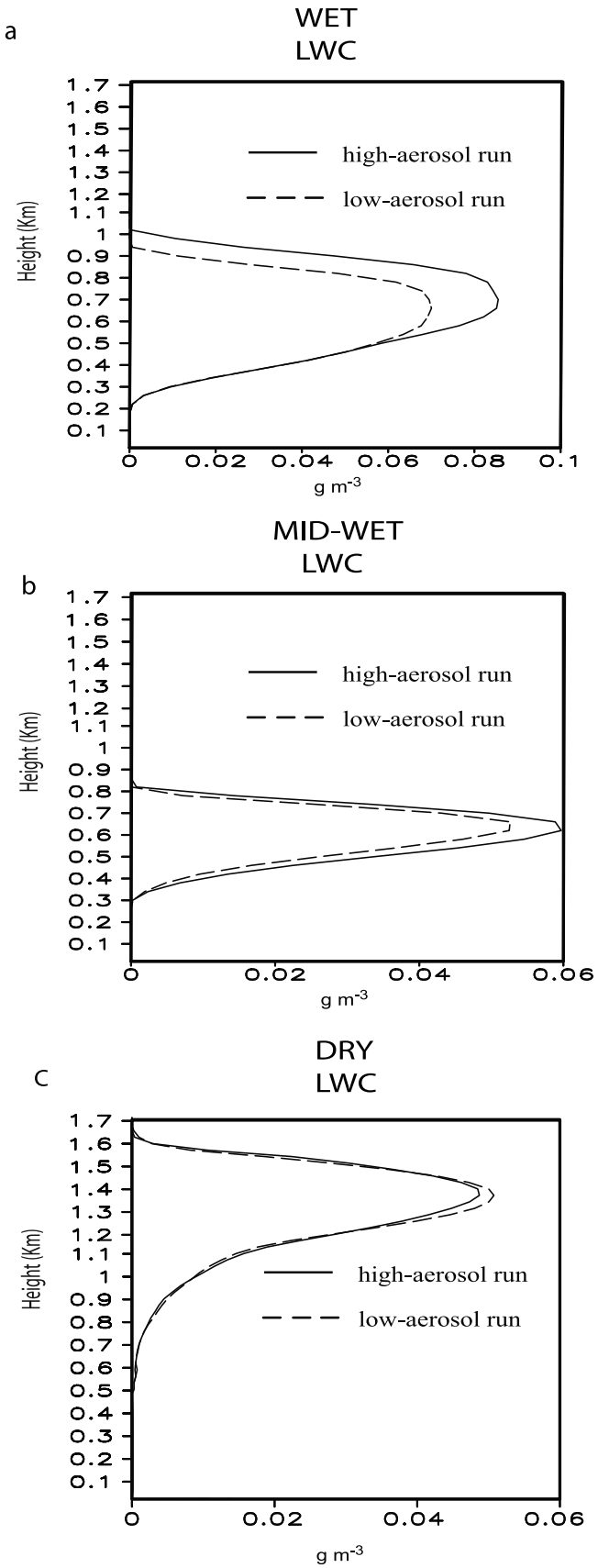

Figure 5. Vertical distribution of time-averaged LWC for (a) WET, (b) MID-WET, and (c) DRY.

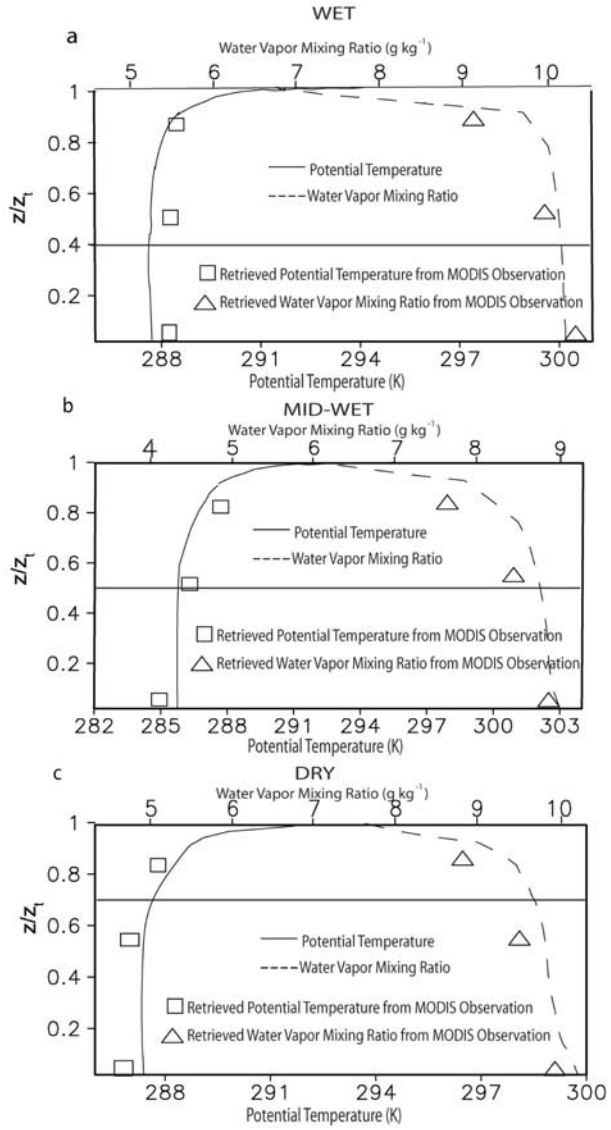

Figure 6. Vertical distribution of time-averaged potential temperature and water vapor mixing ratio for (a) WET, (b) MID-WET, and (c) DRY. Squares (triangles) represent the retrieved potential temperature (water vapor mixing ratio) from the MODIS observation. The solid horizontal line in each figure is the average cloud base height normalized with respect to cloud top height (z_t).

MODIS-observed LWP is less than 10% relative to LWP observed by the MODIS for each case. This demonstrates that the LWPs are simulated reasonably well. Figure 6 shows the time- and domain-averaged vertical profile of potential temperature and water vapor mixing ratio for WET, MID-WET and DRY. The vertical coordinate is in the units of the height normalized with respect to the cloud top height (z_t). Triangles (squares) in Figure 6 are the retrieved potential temperature (water-vapor mixing ratio) from the MODIS observation at the MODIS observation levels. Figure 6 demonstrates that simulated potential temperature and humidity also show a good agreement with the MODIS observations.

[30] Analyses of liquid water budget are performed to examine mechanisms which offset the effects of increased entrainment on LWP to lead to larger LWP at high aerosol in WET and MID-WET. Also, analysis of liquid water budget for DRY is performed to examine the decreasing LWP with increasing aerosols.

5.2. Liquid Water Budget

[31] To elucidate microphysical processes leading to the increase in LWP (and LWC) in WET and MID-WET and the decrease in DRY with increasing aerosols, domain-averaged cumulative source (i.e., condensation) and sinks of cloud liquid (the small-cloud-droplet mode + the large-cloud-droplet mode) and their differences between the high-aerosol run and low-aerosol run (high aerosol−low aerosol) are obtained. For this, a production equation for cloud liquid is integrated over the domain and duration of the simulations. Integrations over the domain and duration of simulation are denoted by brackets:

$$\langle A \rangle = \frac{1}{Lx} \int \int \int \rho_a A dx dz dt \tag{3}$$

where Lx is the domain length (25.4 km), ρ_a is air density and A represents any of the variables in this study. The budget equation for cloud liquid is as follows:

$$\langle \frac{\partial q_c}{\partial t} \rangle = \langle Q_{cond} \rangle - \langle Q_{evap} \rangle - \langle Q_{auto} \rangle - \langle Q_{accr} \rangle \tag{4}$$

Here, q_c is cloud-liquid mixing ratio. Q_{cond}, Q_{evap}, Q_{auto}, and Q_{accr} refer to the rates of condensation, evaporation, autoconversion of cloud liquid to rain, and accretion of cloud liquid by rain, respectively.

[32] Table 2 shows budget numbers of equation (4) for WET, MID-WET and DRY. The high-aerosol run (CDNC-high fixed), low-aerosol run (CDNC-high fixed), high-aerosol run (CDNC-low fixed) and low-aerosol run (CDNC-low fixed) in Table 2 will be discussed in section 5.4. The budget numbers show that condensation and evaporation are two to three orders of magnitude larger than autoconversion and accretion. This indicates that the conversion of cloud liquid (produced by condensation) to rain is highly inefficient. Since all of simulations in WET, MID-WET and DRY (with different environmental and aerosol conditions) show the very low autoconverison and accretion, the extremely inefficient rain formation is fairly robust to environmental and aerosol conditions.

[33] The terminal fall velocity of cloud particles to which sedimentation rate is proportional increases with their increasing size. Also, the sedimentation of cloud mass is mainly controlled by the sedimentation of cloud particles larger than the critical size for collisions around 20−40 μm in radius [*Pruppacher and Klett*, 1997]. Autoconversion and accretion are processes that control the growth of cloud particles after they reached the critical size [*Rogers and Yau*, 1989]. Hence, the small contribution of autoconversion and accretion to LWC implies that the role of sedimentation of cloud particles in the determination of LWC is not as significant as that of condensation and evaporation.

[34] The much larger differences in condensation and evaporation as compared to those in autoconversion and accretion between the high- and low-aerosol runs are simulated here (Table 2). This implies that changes in

Table 2. Domain-Averaged Budget Terms of Cloud Liquid

	$\left\langle \frac{\partial q_c}{\partial t} \right\rangle$ (mm)			Condensation $\langle Q_{cond} \rangle$ (mm)			Evaporation $\langle Q_{evap} \rangle$ (mm)			Autoconversion of Cloud Liquid to Rain $\langle Q_{auto} \rangle$ (mm)			Accretion of Cloud Liquid by Rain $\langle Q_{accr} \rangle$ (mm)		
	WET	MID-WET	DRY	WET	MID-WET	DRY	WET	MID-WET	DRY	WET	MID-WET	DRY	WET	MID-WET	DRY
Low aerosol	0.025	0.038	0.043	0.370	0.123	0.860	0.335	0.083	0.805	0.0030	0.0002	0.0041	0.0070	0.0016	0.0081
High aerosol	0.044	0.049	0.041	0.479	0.145	0.842	0.433	0.095	0.791	0.0001	0.0001	0.0030	0.0020	0.0007	0.0069
Difference (high − low)	0.019	0.011	−0.002	0.109	0.022	−0.018	0.098	0.012	−0.014	−0.0029	−0.0001	−0.0011	−0.0050	−0.0009	−0.0012
Low aerosol (CDNC-high fixed)	0.030	0.047	–	0.449	0.140	–	0.408	0.091	–	0.0032	0.0003	–	0.0075	0.0019	–
High aerosol (CDNC-high fixed)	0.032	0.049	–	0.470	0.143	–	0.432	0.092	–	0.0012	0.0001	–	0.0051	0.0016	–
Difference (high−low)	0.002	0.002	–	0.021	0.003	–	0.024	0.001	–	−0.0020	−0.0002	–	−0.0024	−0.0003	–
Low aerosol (CDNC-low fixed)	0.025	0.040	–	0.362	0.121	–	0.334	0.079	–	0.0009	0.0002	–	0.0020	0.0017	–
High aerosol (CDNC-low fixed)	0.028	0.043	–	0.372	0.125	–	0.342	0.080	–	0.0001	0.0001	–	0.0015	0.0015	–
Difference (high−low)	0.003	0.003	–	0.010	0.004	–	0.008	0.001	–	−0.0008	−0.0001	–	−0.0005	−0.0002	–

condensation and evaporation owing to aerosol increases play much more important roles in the LWP responses to aerosols than those in sedimentation.

[35] Figure 7 shows the time- and domain-averaged vertical distribution of condensation and cloud-mass changes owing to sedimentation for the high- and low-aerosol runs. Cloud mass here is the sum of the mass of all species associated with warm microphysics, i.e., the small-cloud-droplet mode, the large-cloud-droplet mode, and rain. The magnitude of the condensation rate is substantially larger than that of the sedimentation-induced cloud-mass changes for all WET, MID-WET and DRY (Figure 7). Also, the magnitude of difference in the condensation rate between the high- and low-aerosol runs is substantially larger than that in sedimentation-induced mass changes. Hence, as implied by the budget analysis, the LWC and LWP and their responses to aerosols are strongly controlled by condensation and the role of sedimentation in their determination is negligible.

[36] Around cloud top between 0.9 and 1.0 (in the units of the height normalized with respect to the cloud top height) where the intense entrainment occurs, the magnitude of condensation is approximately one to two orders of magnitude larger than that of the sedimentation-induced mass changes (Figure 7). Also, the difference in the condensation rate between the high- and low-aerosol runs is approximately one to two orders of magnitude larger than that in the sedimentation-induced mass changes near cloud top. Cloud liquid is a source of evaporation in subsequent cloud development and evaporation of cloud liquid in downdrafts is one of the important sources of the turbulent kinetic energy (TKE) to entrain warmer and dryer air from above the PBL [*Ackerman et al.*, 2004]. Hence, condensation (controlling the cloud liquid and thus subsequent evaporation) plays more important roles in entrainment and its differences between the high- and low-aerosol runs near cloud top as compared to sedimentation; increased (slightly decreased) condensation and thus evaporation in WET and MID-WET (DRY) lead to increased (slightly decreased) entrainment at high aerosol.

[37] To understand the mechanisms leading to increased condensation in WET and MID-WET and decreased condensation in DRY with increased aerosols, the factors determining condensation are examined.

5.3. Interactions Among CDNC, Condensation, and Dynamics

[38] The equation of mass changes of droplets from the vapor diffusion in this study, integrated over the size distribution, is as follows:

$$\frac{d\overline{m}}{dt} = N_d 4\pi\psi F_{\mathrm{Re}} S \rho_{vsh} \tag{5}$$

where N_d is the CDNC, ψ the vapor diffusivity, and ρ_{vsh} the saturation water vapor mixing ratio. S is the supersaturation, given by $\left(\frac{\rho_{va}}{\rho_{vsh}} - 1\right)$ where ρ_{va} is water vapor mixing ratio. F_{Re} is the integrated product of the ventilation coefficient and droplet diameter which is given by

$$F_{\mathrm{Re}} = \int_0^\infty D f_{\mathrm{Re}} f_{gam}(D) dD \tag{6}$$

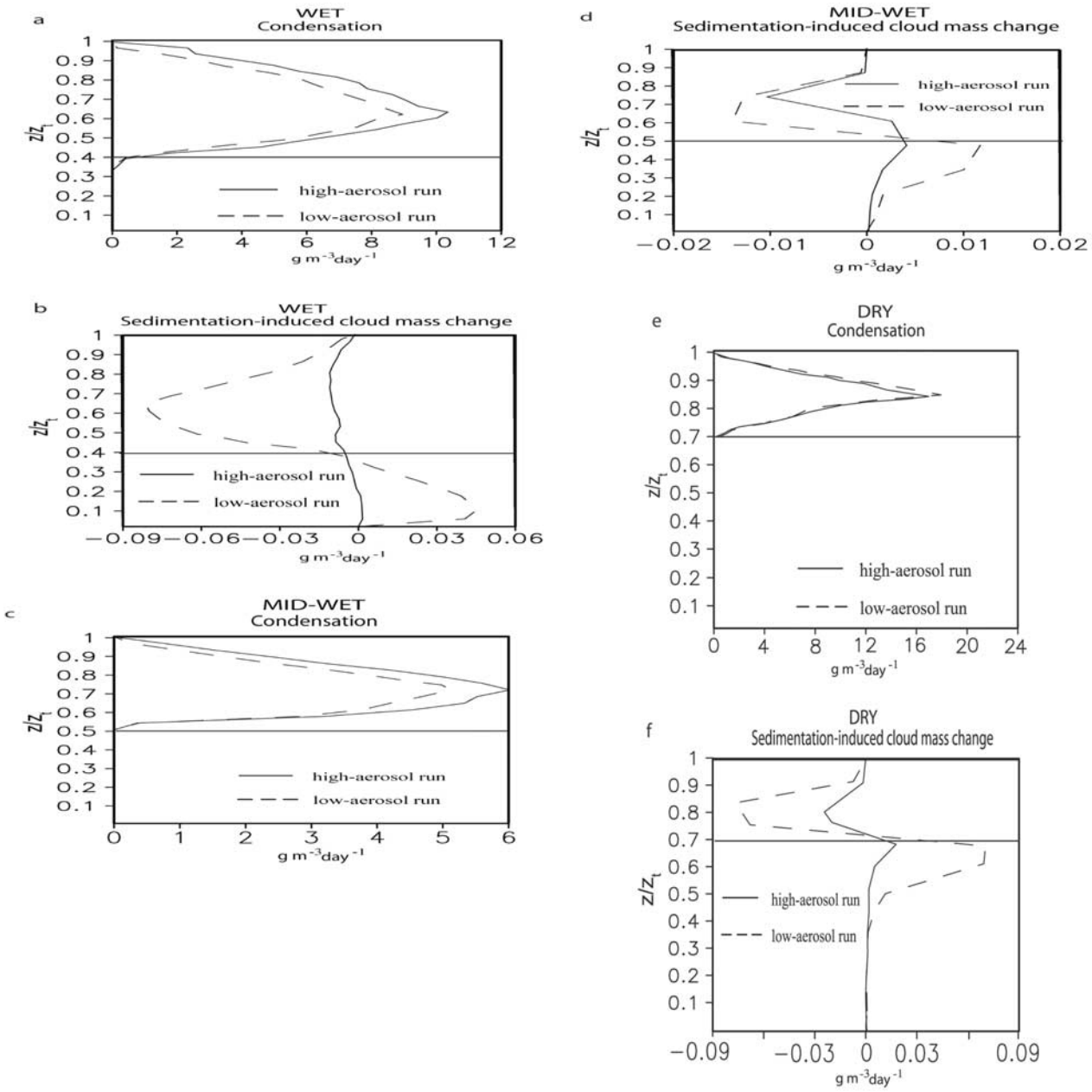

Figure 7. Vertical distribution of time-averaged (a) condensation rate and (b) sedimentation-induced cloud mass change in WET. (c and e) The same as Figure 7a but for MID-WET and DRY, respectively. (d and f) The same as Figure 7b but for MID-WET and DRY, respectively. The solid horizontal line in each figure is the average cloud base height normalized with respect to cloud top height (z_t).

where D is the diameter of droplets, f_{Re} the ventilation coefficient, and $f_{gam_{\nu-1}}$ (D) the distribution function, given by $\frac{1}{\Gamma(\upsilon)}\left(\frac{D}{D_n}\right)^{\nu-1}\frac{1}{D_n}\exp\left(-\frac{D}{D_n}\right)$. f_{Re} is given by $\left[1.0+0.229\left(\frac{v_t D}{V_k}\right)^{0.5}\right]\eta$ where v_t is the terminal velocity and V_k the kinematic viscosity of air and η the shape parameter [*Cotton et al.*, 1982].

[39] Among the variables associated with the condensational growth of droplets in equation (5), differences in the supersaturation and CDNC contribute most to the differences in condensation between the high- and low-aerosol runs. Percentage differences in the other variables are found to be approximately two orders of magnitude smaller than those in supersaturation and CDNC throughout the simulations. Figures 8a, 8d, and 8g show the time series of CDNC and Figures 8b, 8e, and 8h the time series of supersaturation, conditionally averaged over areas where the condensation rate > 0, for WET, MID-WET and DRY, respectively. Figure 8c (Figure 8f) shows the time series of domain-averaged condensation rate for WET (MID-WET) and Figure 8i the time series of domain-averaged cumulative condensation for DRY. The "High-aerosol run × 2" and "low-aerosol run/10" in Figures 8g, 8h, and 8i will be

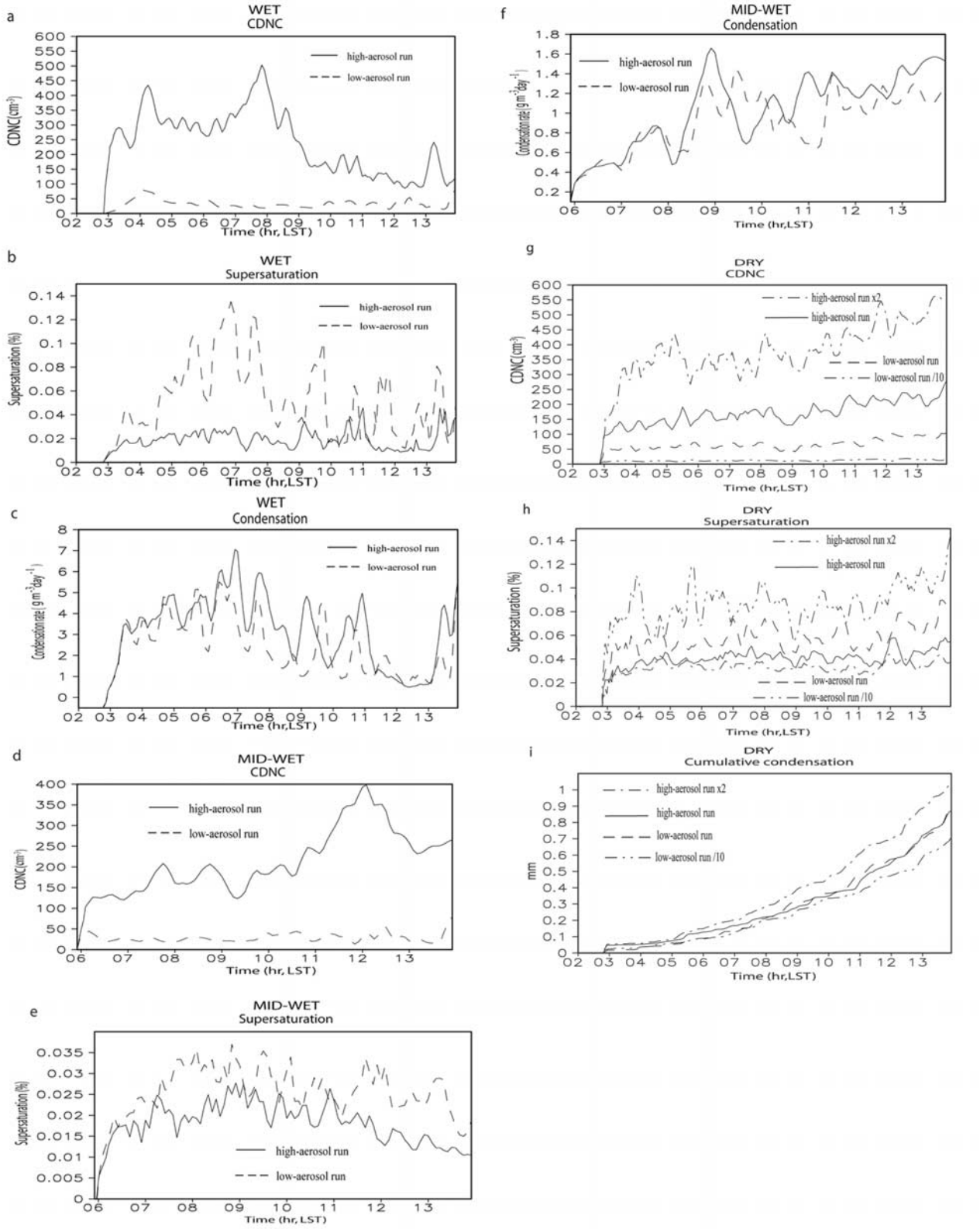

Figure 8. Time series of conditionally averaged (a) CDNC and (b) supersaturation over areas where condensation rate is positive for WET. (c) Time series of domain-averaged condensation rate for WET. (d–f) The same as Figures 8a–8c but for MID-WET. (g and h) The same as Figures 8a and 8b but for DRY. (i) Time series of cumulative condensation for DRY. For the conditional average the grid points with positive values of condensation are collected and the other grid points are excluded. The conditional average is the arithmetic mean of a variable of interest (here CDNC, or supersaturation) over those collected grid points.

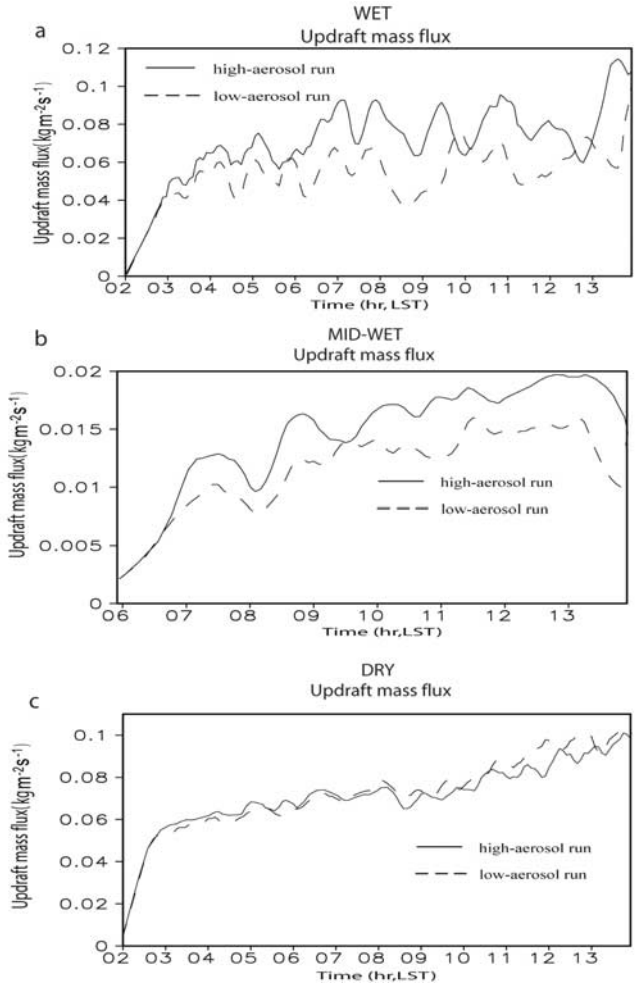

Figure 9. Time series of domain-averaged updraft mass flux (for those whose values are above zero) for (a) WET, (b) MID-WET, and (c) DRY.

described in the following section 5.6. Figures 8b and 8e indicate that supersaturation is generally larger at low aerosol than at high aerosol in both WET and MID-WET. However, the condensation rate is generally higher, leading to larger cumulative condensation at high aerosol than at low aerosol (Figures 8c and 8f). This is ascribed to the larger CDNC (as shown in Figures 8a and 8d) providing a larger surface area for water-vapor condensation at high aerosol compared to that at low aerosol. The effects of the CDNC increase on surface area of droplets and thus condensation compete with the effects of the supersaturation decrease on condensation with increasing aerosols. This leads to the smaller condensation difference than the CDNC and supersaturation differences. The effects of the increased surface area for condensation outweigh the effects of decreased supersaturation, leading to the increase in the condensation in the high-aerosol runs in WET and MID-WET.

[40] Increased condensation provides more condensational heating, and, thereby, intensifies updrafts as shown in Figures 9a and 9b which depict the time series of domain-averaged updraft mass fluxes for WET and MID-WET. Increased updrafts in turn increase condensation, establishing a positive feedback between updrafts and condensation. Therefore, the larger number of cloud droplets providing the larger surface area for condensation plays a critical role in increasing both condensation and updrafts in WET and MID-WET. Note that increased condensation not only increases evaporation, and thus, entrainment, but also increases LWC. In WET and MID-WET, the effects of condensation on LWC outweigh those of evaporation and entrainment, leading to increased LWP at high aerosol. The interactions among CDNC, condensation and dynamics (i.e., updrafts) in WET and MID-WET determine the differences in condensation and thereby the LWP response to aerosols between the high- and low-aerosol runs.

[41] The intensified interactions among condensation and updrafts owing to increased CDNC (Figure 8g) in DRY lead to larger condensation, updrafts (Figures 8i and 9c) and, thereby, LWP in the high-aerosol run than in the low-aerosol run prior to 0800 LST by compensating for lower supersaturation (Figure 8h). The domain-averaged LWPs are 15.12 and 14.55 g m^{-2} in the high- and low-aerosol runs, respectively, prior to 0800 LST. However, Figure 8i shows that condensation rate (indicated by the slope of cumulative condensation) begins to rapidly increase around 0700 LST. As a result of this, cumulative condensation begins to be larger around 0800 LST in the low-aerosol run than in the high-aerosol run in DRY. This leads to larger averaged LWP over entire domain and simulation period at low aerosol than at high aerosol. This indicates that there is a mechanism compensating for the decreased interactions among CDNC, condensation and dynamics in the low-aerosol run in DRY. The analysis of the mechanism is described in the following section 5.5.

5.4. Runs With Different CDNC for Condensation

[42] To isolate the role of the impacts of CDNC (i.e., the surface area of droplets) on condensation in making LWP differences, the high- and low-aerosol runs in WET and MID-WET are repeated with identical CDNC only for condensation but not for the other processes including evaporation. This simulates the LWP differences in the absence of the impacts of the surface area of droplets on condensation. The comparison of these simulations to simulations described in previous sections (i.e., the high- and low-aerosol runs in WET and MID-WET) enables the assessment of the contribution of aerosol and thus CDNC impacts on condensation to the LWP differences.

[43] Two pairs of additional simulations, each of which is composed of the high- and low-aerosol runs, in each of WET and MID-WET are performed. Each pair of simulations adopts the identical CDNC only for condensation; N_d in equation (5) is fixed at a constant value and forced to be the same for the high- and low-aerosol runs, though predicted N_d is allowed to be used in the other processes. The first pair of simulations is referred to as the high-aerosol run (CDNC-high fixed) and low-aerosol run (CDNC-high fixed) in each of WET and MID-WET in Table 2. The high-aerosol run (CDNC-high fixed) and low-aerosol run (CDNC-high fixed) in WET (MID-WET) adopts the averaged CDNC in the high-aerosol run in WET (MID-WET) as a fixed value only for condensation, which is 242 (202) cm^{-3}. The second pair of simulations in WET (MID-WET)

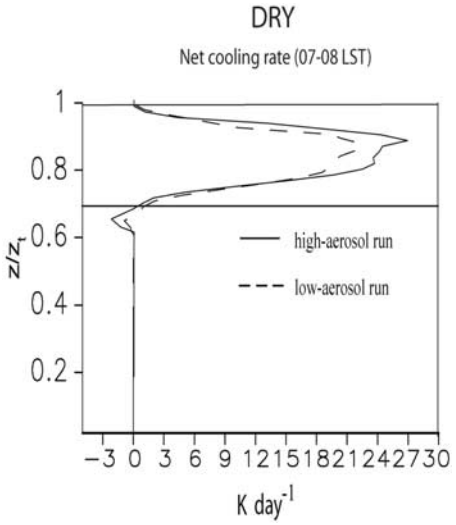

Figure 10. Vertical distribution of time-averaged net cooling rates for DRY over 0700–0800 LST. The solid horizontal line is the average cloud base height normalized with respect to cloud top height (z_t).

adopts the averaged CDNC in the low-aerosol run in WET (MID-WET) as a fixed value only for condensation, which is 39 (40) cm^{-3}, and is referred to as the high-aerosol run (CDNC-low fixed) and low-aerosol run (CDNC-low fixed) in Table 2.

[44] The budget numbers of equation (4) for these additional simulations are shown in Table 2. Time- and domain-averaged LWPs in the high-aerosol run (CDNC-high fixed) and low-aerosol run (CDNC-high fixed) are 47.35 and 46.52 g m^{-2}, respectively, in WET. In MID-WET, the LWPs are 23.55 and 23.30 g m^{-2} in the high-aerosol run (CDNC-high fixed) and low-aerosol run (CDNC-high fixed), respectively. The LWPs in the low-aerosol runs (CDNC-high fixed) increase significantly as compared to LWPs in the low-aerosol runs, resulting in negligible differences in LWP between the high-aerosol run (CDNC-high fixed) and low-aerosol run (CDNC-high fixed) in each of WET and MID-WET. This is mainly due to larger CDNCs in the low-aerosol runs (CDNC-high fixed) than average CDNCs in the low-aerosol runs, leading to increased condensation as compared to that in the low-aerosol runs (Table 2).

[45] The LWP differences between the high-aerosol run (CDNC-low fixed) and low-aerosol run (CDNC-low fixed) are also negligible as compared to those in the high- and low-aerosol runs in each of WET and MID-WET (Table 2). LWPs in the high-aerosol run (CDNC-low fixed) and low-aerosol run (CDNC-low fixed) are 35.90 (18.35) and 35.01 (18.23) g m^{-2}, respectively, in WET (MID-WET). LWPs in the high-aerosol runs (CDNC-low fixed) decreases significantly as compared to LWPs in the high-aerosol runs, resulting in negligible differences in LWP between the high-aerosol run (CDNC-low fixed) and low-aerosol run (CDNC-low fixed) in each of WET and MID-WET (Table 2). This is mainly due to smaller CDNCs in the high-aerosol runs (CDNC-low fixed) than average CDNC in the high-aerosol runs, leading to less condensation than in the high-aerosol runs (Table 2).

[46] These additional simulations indicate that the LWP responses to aerosols can be nearly the same for the high- and low-aerosol runs only by making CDNC for condensation identical. This demonstrates the most crucial role of CDNC impacts on condensation in the LWP responses to aerosols. This also demonstrates that the impacts of aerosols and thus CDNC on the other processes such as the sedimentation of cloud liquid, the conversion of cloud liquid to rain, thus, the sedimentation and evaporation of rain do not play an important role in the LWP responses in thin clouds with the surface precipitation here.

5.5. Effects of Instability on LWP

[47] One of candidates for the mechanism, leading to larger cumulative condensation after 0800 LST in the low-aerosol run than in the high-aerosol run in DRY, is radiative and evaporative cooling around cloud top. Figure 10 shows the net cooling rates averaged over 0700–0800 LST. Figure 10 indicates that cooling is less at low aerosol owing to smaller cloud mass than at high aerosol despite larger warming effects of shortwave radiation owing to larger cloud mass at high aerosol than at low aerosol. Thus, the effect of cloud top cooling favors weaker convection at low aerosol than at high aerosol, indicating that the cooling effect is not likely to contribute to the increase in condensation at low aerosol.

[48] Surface precipitation is absent in DRY. As indicated by *Jiang et al.* [2002], when precipitating particles evaporate completely before reaching the surface, even the slightly increased evaporation of precipitation around the cloud base can cause the increased instability concentrated around the cloud base. When precipitation reaches the surface, the associated cooling tends to stabilize the entire layer below the cloud [*Paluch and Lenschow*, 1991]. Updrafts and downdrafts in the cloud and subcloud layers increase when precipitation does not reach the surface, since its evaporation increases instability around the cloud base [*Feingold et al.*, 1996].

[49] Figures 7f and 11a, depicting domain-averaged sedimentation-induced cloud mass change and rain evaporation in DRY, confirm that precipitation do not reach the surface and that rain evaporates mostly around cloud base (at $z/z_t \sim 0.7$) in both the high- and low-aerosol runs. Increased aerosols in the high-aerosol run delay the formation of precipitation, leading to smaller precipitation and thus its evaporation around cloud base. As shown in Figure 11d, depicting the vertical profile of the time- and domain-averaged rate of conversion of cloud liquid to rain, more droplets are converted to rain at low aerosol. The time- and domain-averaged effective size (in diameter) of cloud droplets is 16 and 10 μm at low aerosol and at high aerosol, respectively. Larger particle size favors more efficient collisions among droplets leading to a higher conversion of droplets to rain. Hence, more rain with higher terminal velocity than droplets precipitate to around the cloud base more at low aerosol than at high aerosol. This in turn leads to larger evaporation of rain just below the cloud base as shown in Figure 11a. Figure 11b, depicting the domain-averaged profile of lapse rate $\frac{d\theta}{dz}$ over 0300–0700 LST, shows that the increase in evaporation below cloud base

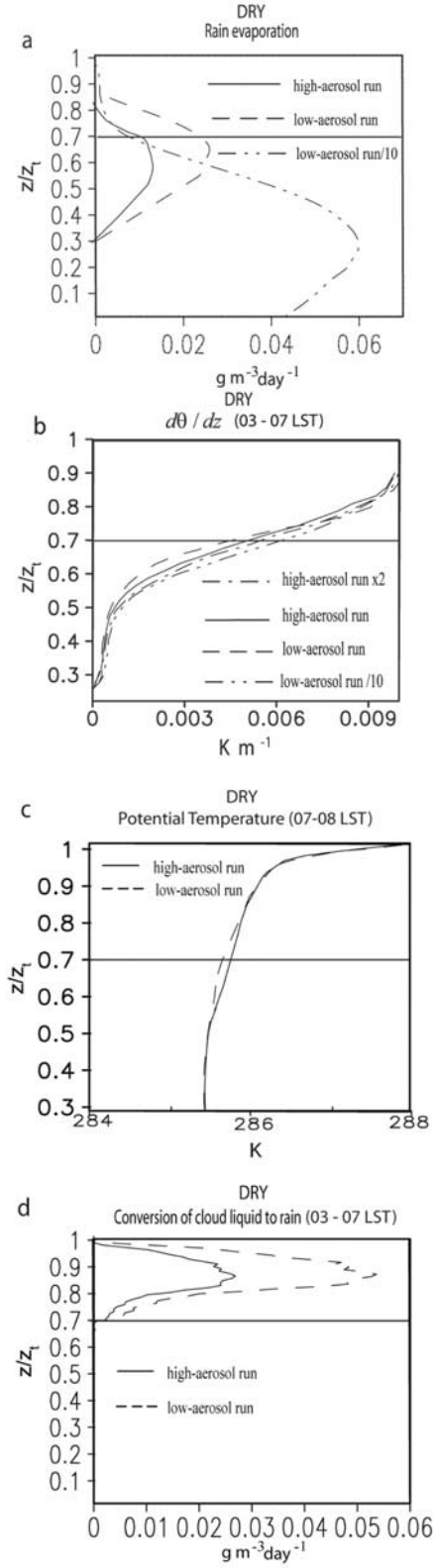

Figure 11. Vertical distribution of the time-averaged (a) rain evaporation rate, (b) $\frac{d\theta}{dz}$, (c) potential temperature, and (d) rate of conversion of cloud liquid to rain for DRY. Figures 11b and 11d are averaged over 0300–0700 LST, and Figure 11c is averaged over 0700–0800 LST. The solid horizontal line in each figure is the average cloud base height normalized with respect to cloud top height (z_t).

leads to larger instability at low aerosol prior to 0700 LST ($\frac{d\theta}{dz}$ is smaller at low aerosol below cloud base). Here, θ is potential temperature. Figure 11c shows the domain-averaged profile of potential temperature over 0700–0800 LST. Smaller $\frac{d\theta}{dz}$ below cloud base leads to lower potential temperature at low aerosol around cloud base. This larger instability drives stronger updrafts and downdrafts in the PBL over 0700–0008 LST in the low-aerosol run as shown in Figures 12a and 12b. Increased positive and negative buoyancy associated with stronger updrafts and downdrafts, respectively, drive an increase in the variance of vertical air motion ($\overline{w'w'}$) in the low-aerosol run than in the high-aerosol run as shown in Figure 12c depicting averaged $\overline{w'w'}$ over 0700–0800 LST. Stronger vertical motion leads to the rapidly increasing condensation around 0700 LST and then to larger cumulative condensation at 0800 LST at low aerosol than at high aerosol (Figure 8i).

[50] Aerosol effects on the instability around cloud base in DRY compete with interactions among CDNC, conden-

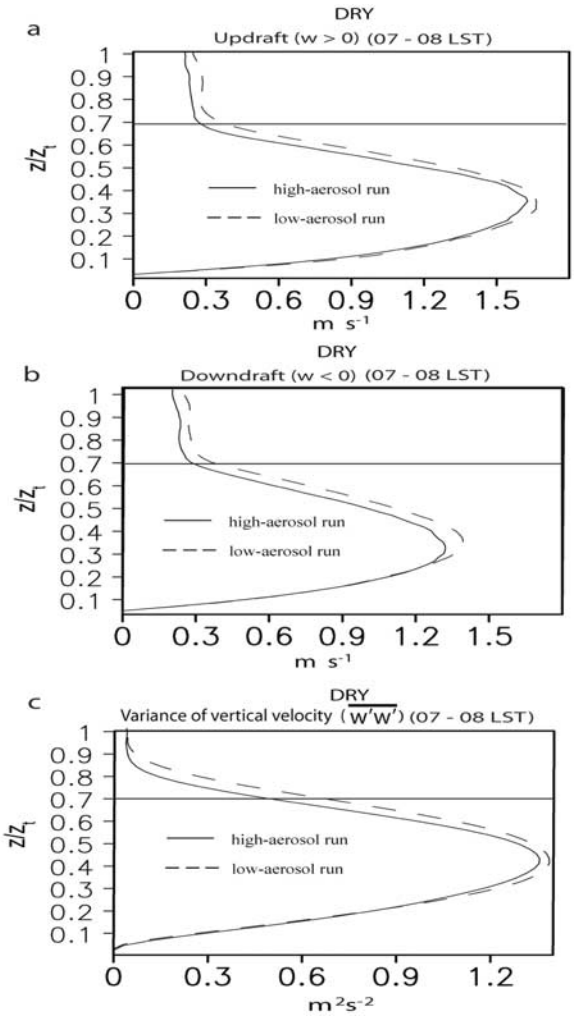

Figure 12. Vertical distribution of domain-averaged (a) updrafts (w > 0), (b) downdrafts (w < 0), and (c) variance of vertical velocity ($\overline{w'w'}$) averaged over 0700–0800 LST for DRY. The solid horizontal line in each figure is the average cloud base height normalized with respect to cloud top height (z_t).

sation and dynamics; increased aerosols not only decrease the instability around cloud base but also increase interactions among CDNC, condensation and dynamics. The effects of decreased instability outweigh those of the intensified interactions among CDNC, condensation and dynamics with increased aerosols, leading to smaller LWP in the high-aerosol run than in the low-aerosol run. Next, we discuss additional simulations performed to examine the effects of the competition between interactions (among CDNC, condensation and dynamics) and instability (around cloud base) in determining the change in LWP in more detail.

5.6. Runs With Different Aerosols

[51] Another experiment for DRY is performed with the same model setup as in the high-aerosol run but with increased background aerosols by a factor of 2 as compared to that in the high-aerosol run to examine the competition between interactions (among CDNC, condensation and dynamics) and instability (around cloud base) in DRY. This experiment is referred to as "high-aerosol run $\times$ 2" henceforth. Figure 8i shows that condensation in this experiment is higher, leading to larger LWP (32.11 g m^{-2}) than that in the low-aerosol run (30.21 g m^{-2}). Although the supersaturation in this experiment is lower, condensation is larger than that in the low-aerosol run owing to the larger CDNC (Figures 8g, 8h, and 8i). In the high-aerosol run, the CDNC increase is not large enough to compensate for the decreased supersaturation through the interactions among CDNC, condensation and dynamics, leading to a smaller LWP than in the low-aerosol run in DRY. However, in the simulation with aerosols 2 times larger than those in the high-aerosol run in DRY, increased CDNC is large enough to compensate for the decreased supersaturation, leading to larger condensation than that in the low-aerosol run. The difference in the instability averaged over 0300–0700 LST around cloud base between this simulation and the low-aerosol run is larger than that between the high-aerosol run and low-aerosol run in DRY (Figure 11b). This also holds if the instability is averaged over the whole simulation period. Despite this larger decrease in the instability around the cloud base in this experiment than that in the high-aerosol run as compared to the instability in the low-aerosol run, increased interactions between CDNC and dynamics lead to larger condensation (Figure 8i) and LWP.

[52] Increased aerosols increase the interactions between CDNC and dynamics as well as decrease the instability around cloud base. The LWP response to aerosols is mostly controlled by the competition between these interactions and instability, while the sedimentation does not play an important role in the LWP response in DRY as in WET and MID-WET.

[53] To examine the role of rain evaporation in instability and thereby condensation in the case where precipitation reaches the surface, the fourth simulation for DRY is performed. This simulation is carried out with the same model setup as in the low-aerosol run in DRY but with reduced background aerosols by a factor of 10 as compared to those in the low-aerosol run in DRY and referred to as the "low-aerosol run/10" henceforth. Owing to reduced aerosols, CDNC reduces, leading to more conversion of cloud liquid to rain as compared to those in the low-aerosol run in DRY. This induces more evaporation of rain in the subcloud layer than in the low-aerosol run as shown in Figure 11a. Figure 11a indicates rain reaches the surface in the low-aerosol run/10. Figure 11b shows the instability averaged over 0300–0700 LST in this run is smaller (this also holds for the instability averaged over the entire simulation period) than in the high-aerosol run. This indicates that the increased evaporation of precipitating particles does not lead to increased instability when precipitation reaches the surface as reported by *Paluch and Lenschow* [1991]. Also, the reduced CDNC reduces the interactions among CDNC, condensation and dynamics. Reduced instability and those interactions lead to smaller condensation (and thus LWP) than in the high-aerosol run (Figure 8i). Domain-averaged LWP is 25.92 and 29.70 g m^{-2} in the low-aerosol run/10 and high-aerosol run. When precipitation reaches the surface, the effect of decreasing aerosols on the instability acts to reduce condensation and LWP.

5.7. Buoyancy Fluxes

[54] Figures 13a and 13b show the vertical distribution of time- and domain-averaged buoyancy fluxes ($\overline{w'\theta_v'}$) in WET and MID-WET, respectively. Here, w is vertical velocity and θ_v virtual potential temperature. Figures 13c and 13d show the vertical distribution of domain-averaged buoyancy fluxes in DRY. Figures 13c and 13d are averaged over 0300–0800 and 0800–1400 LST, respectively. In all cases, buoyancy fluxes decrease almost linearly from the surface. However, unlike in WET and MID-WET, buoyancy fluxes are negative from around the middle of subcloud layer to just below the cloud base in DRY.

[55] Just above cloud base, buoyancy fluxes jump abruptly to a high positive value owing to the onset of condensation and evaporation of cloud liquid; as one goes higher in cloud, buoyancy fluxes decrease to negative values around cloud top owing to entrainment. Greater condensation and evaporation at high aerosol lead to higher buoyancy fluxes in the cloud layer in WET and MID-WET. There are no layers of negative buoyancy fluxes below the clouds and negative buoyancy fluxes around cloud top are not substantial in WET and MID-WET. These indicate that subcloud and cloud layers can be considered coupled in WET and MID-WET, according to the buoyancy integral ratio (BIR) of *Bretherton and Wyant* [1997, equation (14)]. The BIR is defined as the ratio of integral of magnitude of buoyancy fluxes over the regions of negative buoyancy below cloud base to integral of buoyancy fluxes over all other regions. *Bretherton and Wyant* [1997] considered PBL decoupled when the BIR exceeds 0.15. Simulations in DRY show BIR of $\sim$0.08. Hence, despite the presence of negative buoyancy fluxes in the subcloud layer, BIR indicates subcloud and cloud layers can be considered coupled in DRY.

[56] At the first time segment in DRY, the high-aerosol run shows larger fluxes owing to more condensation. However, at the second time segment, the low-aerosol run show larger fluxes as a result of larger cloud base instability and thus condensation; $\sim$20% increase in the fluxes is simulated.

5.8. Radiation Budget

[57] It is found that the variation of longwave flux at the top and the base of the atmosphere and of upward short-

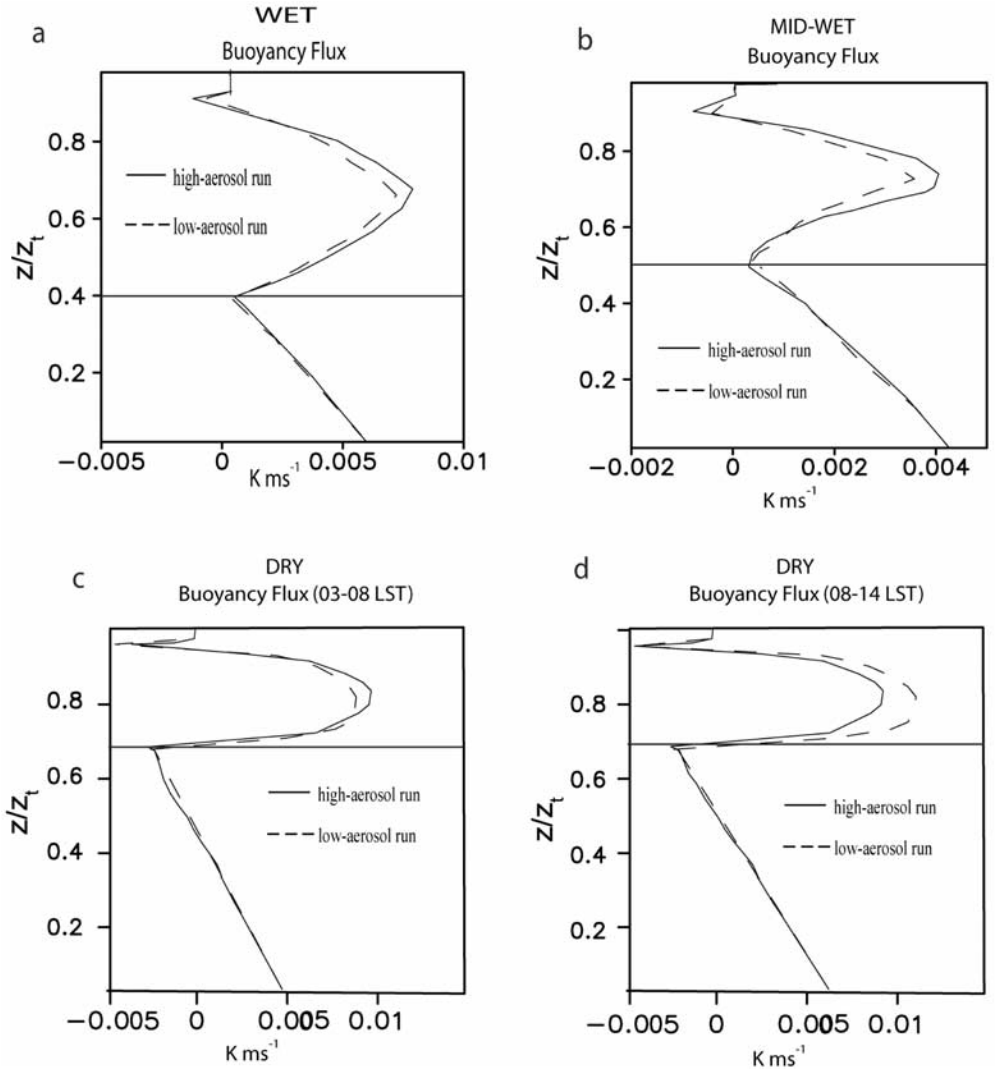

Figure 13. Vertical distribution of the time-averaged buoyancy flux ($\overline{w'\theta_v'}$) for (a) WET and (b) MID-WET. (c and d) The vertical distribution of the time-averaged buoyancy flux over 0300–0800 and 0800–1400 LST, respectively, for DRY. The solid horizontal line in each figure is the average cloud base height normalized with respect to cloud top height (z_t).

wave flux at the base of the atmosphere owing to aerosol changes are negligible as compared to that of upward and downward shortwave fluxes at the top and base of the atmosphere, respectively. Also, downward shortwave flux at the top of the atmosphere is identical for the high- and low-aerosol runs. Hence, only upward and downward shortwave fluxes at the top and base of the atmosphere, respectively, are presented in Table 3 (↑ and ↓ denote upward and downward fluxes, respectively). In Table 3, SW represents shortwave flux.

[58] The low-aerosol run has lower TOA upward SW (for radiation, TOA is at the level of 0.01 hPa) than the high-aerosol run; more SW is reflected in the high-aerosol run than in the low-aerosol run by 33.0 and 7.0 W m^{-2} in WET and MID-WET, respectively. More SW is reflected in the high-aerosol run than in the low-aerosol run by 3.2 W m^{-2} in DRY despite smaller LWP and cloud fraction (time-averaged cloud fractions are 0.98 (0.99) at high (low)

Table 3. Time- and Area-Averaged Upward Shortwave Flux at the Top of the Atmosphere and Downward Shortwave Flux at the Base of the Atmosphere[a]

	WET (W m^{-2})	MID-WET (W m^{-2})	DRY (W m^{-2})
	SW↑ at TOA		
Low aerosol	176.8	145.9	193.4
High aerosol	209.8	152.9	196.6
Difference (high−low)	33.0	7.0	3.2
	SW↓ at SFC		
Low aerosol	588.6	753.5	582.2
High aerosol	547.5	744.9	578.3
Difference (high−low)	−41.1	−8.6	−3.9

[a]Upward and downward pointing arrows denote upward and downward radiation, respectively. SW, shortwave flux; TOA, top of the atmosphere; SFC, base of the atmosphere.

aerosol in DRY). This is because the effect of smaller sizes of droplets on the reflection of SW outweighs that of smaller LWP and cloud fraction at high aerosol.

[59] Downward SW at the base of the atmosphere has a higher value in the low-aerosol run than in the high-aerosol run by 41.1, 8.6, and 3.9 W m^{-2} in WET, MID-WET and DRY, respectively. More absorption of SW at high aerosol leads to larger differences in the downward SW at the base of the atmosphere than that in outgoing SW at the top of the atmosphere.

[60] In-cloud average effective droplet diameters are 14 (20) and 9 (11) μm at high (low) aerosol in WET and MID-WET, respectively; the high-aerosol runs have smaller droplets mainly owing to larger CDNC. Time-averaged cloud fractions are 0.98 (0.96) and 0.98 (0.97) at high (low) aerosol in WET and MID-WET, respectively. Larger LWP and smaller droplets owing to increased condensation and CDNC in tandem with greater cloud fraction at high aerosol lead to larger reflection and absorption of downward SW in WET and MID-WET. The effects of smaller droplet size on the reflection of downward SW at high aerosol lead to larger reflection of downward SW (and more outgoing SW at the top of the atmosphere and less SW reaching the surface) in DRY.

6. Summary and Conclusion

[61] Aerosol-cloud interactions in thin stratocumulus clouds with LWP < 50 g m^{-2} over the North Atlantic in the summer in 2002 were simulated using a CSRM coupled with a double-moment microphysics. Stratocumulus clouds over three regions with different humidity around the top of boundary layer were selected. Present-day and preindustrial aerosols were prescribed to those three cases of clouds to examine aerosol effects on LWP.

[62] WET and MID-WET in this study showed increased LWP at high aerosol. The sedimentation of cloud particles played a negligible role in the LWP responses to aerosols. Instead, it was found that feedbacks among CDNC, condensation and dynamics led to increased LWP at high aerosol in WET and MID-WET by compensating for the effect of increased entrainment near cloud top. The role of different sedimentation near cloud top in different entrainment between the high- and low-aerosol runs was also negligible as compared to that of those feedbacks. Increased cloud liquid near cloud top mostly owing to these intensified feedbacks provided a larger source of evaporative cooling at high aerosol than at low aerosol in WET and MID-WET. This contributed more to increased entrainment at high aerosol than sedimentation changes owing to aerosols in WET and MID-WET.

[63] *Khairoutdinov and Kogan* [2000] indicated that the sensitivity of the conversion of cloud liquid to rain to varying CDNC was weaker at low LWC than at high LWC. This implies that the sensitivity of the growth of droplets through collisions with other particles (controlling the conversion of cloud liquid to rain) and thus the sensitivity of sedimentation to aerosol changes (leading to CDNC changes) is weaker at low LWC. The variation of the conversion of cloud droplets to rain with varying aerosols was not large enough to make a significant difference in the sedimentation of cloud particles among simulations with low LWC here (see Figures 5 and 7), as also implied by the study of *Khairoutdinov and Kogan* [2000]. This led to a negligible role of sedimentation in the response of LWP and entrainment to aerosols.

[64] The negligible role of sedimentation is at odds with previous studies such as *Ackerman et al.* [2004] who found that sedimentation determined the LWP response to aerosols. One of differences between this study and that of *Ackerman et al.* [2004] is that *Ackerman et al.* [2004] simulated relatively thick clouds with the LWP > 70 g m^{-2}. The variation of sedimentation with increasing aerosols is larger in these thick clouds of *Ackerman et al.* [2004] than that in the thin clouds here. This can be explained by the dependence of the variation of sedimentation on the level of LWC described in the work of *Khairoutdinov and Kogan* [2000]. Thus, it appears that the thickness of clouds defined by the level of LWC (and thus LWP) determines whether sedimentation or those feedbacks play a crucial role in the LWP response. However, *Ackerman et al.* [2004] simulated nocturnal clouds, while this study simulated the diurnal evolution of clouds. Nocturnal clouds evolve with different environmental factors (e.g., radiation and the PBL stratification) as compared to the clouds simulated here. Hence, it is hard to ascribe the cause of the difference in the mechanism of the LWP responses solely to the level of LWP. The understanding of more possible factors leading to the difference deserves further study.

[65] In clouds with no surface precipitation in DRY, the larger sedimentation of rain at low aerosol (with preindustrial aerosols) than at high aerosol (with present-day aerosols) developed a larger instability around cloud base. This led to increased updraft motions and thereby increased condensation at low aerosol. Increased instability around cloud base at low aerosol with preindustrial aerosols contributed to the larger LWP by compensating for the decreased feedbacks among CDNC, condensation and dynamics. In an additional simulation with aerosols increased by a factor of 2 over those in the run with the present-day aerosols for DRY, LWP was larger than that in the low-aerosol run with preindustrial aerosols. This is because the increased CDNC as compared to that in the run with present-day aerosols intensified the feedbacks among CDNC, condensation and dynamics. This offset the effect of decreased instability on the LWP owing to decreased sedimentation of rain, leading to an increased LWP as compared to that in the run with preindustrial aerosols. When aerosols decreased by a factor of 10 from those in the run with preindustrial aerosols, LWP decreased as compared to those in the run with present-day aerosols. Feedbacks among CDNC, condensation and dynamics weakened in this experiment as compared to those in the run with preindustrial aerosols. Also, precipitation reached the surface in this experiment, stabilizing the entire boundary layer below the cloud. This led to a decreased LWP with decreased aerosols in the low-aerosol run/10, which is different from the increased LWP with decreased aerosols in the low-aerosol run with no surface precipitation.

[66] Additional simulations with a fixed CDNC only for condensation showed that aerosol effects on the processes (including evaporation) other than condensation played a negligible role in the LWP responses to aerosols in all cases

here, despite differences in the environmental temperature and humidity distributions in the initial conditions and forcings among WET, MID-WET and DRY. This confirmed that the variation of condensation predominantly determined the LWP responses regardless of different environmental temperature and humidity distributions among the three cases. Thus, the linkage of those responses to the temperature and humidity conditions in and above the PBL is weak in the thin clouds here. Instead, they are strongly linked to CDNC levels and the presence of the surface precipitation, controlling condensation. This suggests that the qualitative nature of results presented here is fairly robust to the background temperature and humidity conditions.

[67] The coarse spatial resolutions employed in climate models are not able to resolve the interactions among CDNC, condensation, and updrafts in the cloud layer and the instability around cloud base, which play important roles in aerosol effects on LWP in thin clouds here. Hence, it is necessary to develop parameterizations that are able to consider the effects of these interactions and instability on the LWP variation with aerosols. So far, in general, parameterizations for the representation of the LWP variation with aerosols have simply relied on changes in the autoconversion of cloud liquid and sedimentation of cloud liquid and rain with varying aerosols in climate models. They do not take into account feedbacks between microphysics, dynamics, and the instability. This can contribute to a large uncertainty in the estimation of radiative forcing associated with aerosol indirect effects, considering the significant coverage of thin clouds and the strong sensitivity of the radiative fluxes to the LWP variation in thin clouds as reported in previous studies [e.g., *Turner et al.*, 2007; *McFarlane and Evans*, 2004; *Shupe and Intrieri*, 2004; *Marchand et al.*, 2003]. Also, most of climate models and some of CSRMs have adopted saturation adjustment schemes which are not able to predict supersaturation and to thereby consider the effects of changes in the surface area of cloud particles for the calculation of condensation. Hence, using a saturation adjustment scheme prevents the simulation of the changing competition between supersaturation and the surface area of cloud particles with increasing aerosols. Thus, this prevents the simulation of varying interactions among CDNC, condensation, and dynamics with aerosols, which can lead to incorrect assessments of aerosol effects on thin clouds. Therefore, microphysics parameterizations, able to predict particle mass and number, and thereby, surface area, coupled with a prediction of supersaturation, need to be implemented into climate models for a correct assessment of aerosol effects on thin clouds. Also, for thin clouds with no surface precipitation, those parameterizations should be able to take into account rain evaporation and its effects on the instability around cloud base.

[68] In this study, identical surface fluxes from observations were prescribed for high- and low-aerosol runs for each humidity case. Therefore, surface fluxes did not contribute to different instability and feedbacks among CDNC, condensation and dynamics. We focused on how aerosols affect thin clouds for an identical net heat and moisture supplied to or removed from the domain by the large-scale flow and surface fluxes. Although feedbacks from differences in clouds onto the large-scale flow and surface fluxes cannot be captured by this design, this isolates interactions among aerosols, microphysics, local dynamics and instability and enables the identification of microphysics–aerosol interactions on the scale of cloud systems.

[69] *Guo et al.* [2008] indicated that the cloud development was sensitive to the vertical resolution. However, *Guo et al.* [2008] found that basic features of the integrations (e.g., the inversion height, LWP and cloud top radiative cooling) were similar for vertical resolutions of 40 m or finer. Consistent with the finding of *Guo et al.* [2008], an additional set of simulations with a vertical resolution of 15 m for WET, MID-WET and DRY show nearly identical results to those with the resolution of 40 m below the top of the PBL. This indicates that the qualitative nature of results here is robust to the vertical resolution.

[70] Droplet (equivalent to cloud liquid in this study) sedimentation can play an important role in cloud development [*Ackerman et al.*, 2004], since it can affect entrainment around cloud top significantly. The high- and low-aerosol runs were repeated with no cloud-liquid sedimentation to examine the role of droplet sedimentation in results here. These simulations showed that similar variation of LWP with aerosols to simulations with cloud-liquid sedimentation through mechanisms described in the section 5. This demonstrates that the qualitative nature of results of this study does not depend on the presence of droplet sedimentation.

[71] The generalization of the results reported here requires further investigation. The three sets of simulations examined here are too limited to form a generalized basis for determining the effects of aerosol on thin stratiform clouds and, thus, their parameterizations for large-scale or climate models. More case studies of thin stratiform clouds developing under various environmental conditions are needed to establish the generalization of the results reported here. The second AIE is known to be inextricably entangled with the environmental conditions such as the humidity, large-scale subsidence, sea surface temperature (SST), and surface sensible and latent heat fluxes [*Jiang et al.*, 2002; *Ackerman et al.*, 2004; *Guo et al.*, 2007]. Hence, aerosol–cloud interactions in thin clouds may vary with these environmental factors and this needs to be addressed in future studies.

[72] **Acknowledgments.** The authors wish to thank Derek Posselt for providing GCE coupled with double-moment microphysics used here and in valuable discussions. This paper was prepared under U.S. Department of Energy ARM program (DE FG02 97 ER62370).

References

Ackerman, A. S., M. P. Kirkpatrick, D. E. Stevens, and O. B. Toon (2004), The impact of humidity above stratiform clouds on indirect aerosol climate forcing, *Nature*, *432*, 1014–1017, doi:10.1038/nature03174.

Albrecht, B. A. (1989), Aerosols, cloud microphysics, and fractional cloudiness, *Science*, *245*, 1227–1230, doi:10.1126/science.245.4923.1227.

Bretherton, C. S., and M. C. Wyant (1997), Moisture transport, lower-tropospheric stability, and decoupling of cloud-topped boundary layers, *J. Atmos. Sci.*, *54*, 148–167.

Chou, M.-D., and L. Kouvaris (1991), Calculations of transmission functions in the IR CO_2 and O_3 bands, *J. Geophys. Res.*, *96*, 9003–9012.

Chou, M.-D., and M. J. Suarez (1999), A shortwave radiation parameterization for atmospheric studies, *NASA TM-104606*, vol. 15, 40 pp.

Chou, M.-D., W. Ridgway, and M.-H. Yan (1995), Parameterizations for water vapor IR radiative transfer in both the middle and lower atmospheres, *J. Atmos. Sci.*, *52*, 1159–1167, doi:10.1175/1520-0469(1995)052<1159:PFWVIR>2.0.CO;2.

Collins, W. D., et al. (2006a), The Community Climate System Model: CCSM3, *J. Clim.*, *19*, 2122–2143, doi:10.1175/JCLI3761.1.

Collins, W. D., et al. (2006b), The formulation and atmospheric simulation of the community atmosphere model version 3 (CAM3), *J. Clim.*, *19*, 2144–2161, doi:10.1175/JCLI3760.1.

Cotton, W. R., M. A. Stephens, T. Nehrkorn, and G. J. Tripoli (1982), The Colorado State University three-dimensional cloud/mesoscale model. Part II: An ice phase parameterization, *J. Rech. Atmos.*, *16*, 295–319.

Donner, L. J., C. J. Seman, and R. S. Hemler (1999), Three-dimensional cloud-system modeling of GATE convection, *J. Atmos. Sci.*, *56*, 1885–1912, doi:10.1175/1520-0469(1999)056<1885:TDCSMO>2.0.CO;2.

Feingold, G., and A. J. Heymsfield (1992), Parameterizations of condensational growth of droplets for use in general circulation models, *J. Atmos. Sci.*, *49*, 2325–2342, doi:10.1175/1520-0469(1992)049<2325:POCGOD>2.0.CO;2.

Feingold, G., S. Tzivion, and Z. Levin (1988), Evolution of raindrop spectra. part I: Solution to the stochastic collection/breakup equation using the method of moments, *J. Atmos. Sci.*, *45*, 3387–3399, doi:10.1175/1520-0469(1988)045<3387:EORSPI>2.0.CO;2.

Feingold, G., B. Stevens, W. R. Cotton, and A. S. Frisch (1996), The relationship between drop in-cloud residence time and drizzle production in numerically simulated stratocumulus clouds, *J. Atmos. Sci.*, *53*, 1108–1122, doi:10.1175/1520-0469(1996)053<1108:TRBDIC>2.0.CO;2.

Feingold, G., W. Cotton, S. Kreidenweis, and J. Davis (1999), The impact of giant cloud condensation nuclei on drizzle formation in stratocumulus: Implications for cloud radiative properties, *J. Atmos. Sci.*, *56*, 4100–4117, doi:10.1175/1520-0469(1999)056<4100:TIOGCC>2.0.CO;2.

Forster, P., et al. (2007), Changes in atmospheric constituents and in radiative forcing, in *Climate Change 2007: The Physical Science Basis, Contribution of Working Group I to the Fourth Assessment Report of the Intergovernmental Panel on Climate Change*, edited by S. Solomon et al., pp. 130–234, Cambridge Univ. Press, New York.

Grabowski, W. W., X. Wu, and M. W. Moncrieff (1996), Cloud resolving modeling of tropical cloud systems during phase III of GATE. part I: Two-dimensional experiments, *J. Atmos. Sci.*, *53*, 3684–3709, doi:10.1175/1520-0469(1996)053<3684:CRMOTC>2.0.CO;2.

Guo, H., J. E. Penner, M. Herzog, and S. Xie (2007), Investigation of the first and second aerosol indirect effects using data from the May 2003 Intensive Operational Period at the Southern Great Plains, *J. Geophys. Res.*, *112*, D15206, doi:10.1029/2006JD007173.

Guo, H., Y. Liu, P. H. Daum, X. Zeng, X. Li, and W.-K. Tao (2008), Effects of model resolutions on entrainment (inversion heights), cloud-radiation interactions, and cloud radiative forcing, *Atmos. Chem. Phys. Disc.*, *8*, 20,399–20,425.

Hall, W. (1980), A detailed microphysical model within a two-dimensional dynamic framework: Model description and preliminary results, *J. Atmos. Sci.*, *37*, 2486–2507, doi:10.1175/1520-0469(1980)037<2486:ADMMWA>2.0.CO;2.

Herzog, M., D. Weisenstein, and J. E. Penner (2004), An aerosol module for global chemical transport models: Model description, *J. Geophys. Res.*, *109*, D18202, doi:10.1029/2003JD004405.

Heymsfield, A. J., and R. M. Sabin (1989), Cirrus crystal nucleation by homogeneous freezing of solution droplets, *J. Atmos. Sci.*, *46*, 2252–2264, doi:10.1175/1520-0469(1989)046<2252:CCNBHF>2.0.CO;2.

Ito, A., and J. E. Penner (2005), Estimates of CO emissions from open biomass burning in southern Africa for the year 2000, *J. Geophys. Res.*, *110*, D19306, doi:10.1029/2004JD005347.

Jiang, H., G. Feingold, and W. R. Cotton (2002), Simulations of aerosol-cloud-dynamical feedbacks resulting from entrainment of aerosol into the marine boundary layer during the Atlantic Stratocumulus Transition Experiment, *J. Geophys. Res.*, *107*(D24), 4813, doi:10.1029/2001JD001502.

Khairoutdinov, M., and Y. Kogan (2000), A new cloud physics parameterization in a large-eddy simulation model of marine stratocumulus, *Mon. Weather Rev.*, *128*, 229–243, doi:10.1175/1520-0493(2000)128<0229:ANCPPI>2.0.CO;2.

Klemp, J. B., and R. Wilhelmson (1978), The simulation of three-dimensional convective storm dynamics, *J. Atmos. Sci.*, *35*, 1070–1096, doi:10.1175/1520-0469(1978)035<1070:TSOTDC>2.0.CO;2.

Kratz, D. P., M.-D. Chou, M.-H. Yan, and C.-H. Ho (1998), Minor trace gas radiative forcing calculations using the k-distribution method with one-parameter scaling, *J. Geophys. Res.*, *103*, 31,647–31,656, doi:10.1029/1998JD200009.

Krueger, S. K., R. T. Cederwall, S. C. Xie, and J. J. Yio (1999), GCSS Working Group 4 Model Intercomparison—Procedures for Case 3: Summer 1997 ARM SCM IOP, technical report, 15 pp., GEWEX Cloud Syst. Study, Univ. of Utah, Salt Lake City. (Available at ftp://ftp.met.utah.edu/pub/skrueger/gcss_wg4_case3/gcss-wg4-case3-doc.pdf)

Liu, X., and J. E. Penner (2002), Effect of Mount Pinatubo H_2SO_4/H_2O aerosol on ice nucleation in the upper troposphere using a global chemistry and transport model, *J. Geophys. Res.*, *107*(D12), 4141, doi:10.1029/2001JD000455.

Liu, X., J. E. Penner, and M. Herzog (2005), Global modeling of aerosol dynamics: Model description, evaluation and interactions between sulfate and non-sulfate aerosols, *J. Geophys. Res.*, *110*, D18206, doi:10.1029/2004JD005674.

Long, A. (1974), Solutions to the droplet collection equation for polynomial kernels, *J. Atmos. Sci.*, *31*, 1040–1052, doi:10.1175/1520-0469(1974)031<1040:STTDCE>2.0.CO;2.

Marchand, R., T. Ackerman, E. R. Westwater, S. A. Clough, K. Cady-Pereira, and J. C. Liljegren (2003), An assessment of microwave absorption models and retrievals of cloud liquid water using clear-sky data, *J. Geophys. Res.*, *108*(D24), 4773, doi:10.1029/2003JD003843.

McFarlane, S. A., and K. F. Evans (2004), Clouds and shortwave fluxes at Nauru. part I: Retrieved cloud properties, *J. Atmos. Sci.*, *61*, 733–744, doi:10.1175/1520-0469(2004)061<0733:CASFAN>2.0.CO;2.

Moeng, C.-H., P. P. Sullivan, and B. Stevens (1999), Including radiative effects in an entrainment rate formula for buoyancy-driven PBLs, *J. Atmos. Sci.*, *56*, 1031–1049, doi:10.1175/1520-0469(1999)056<1031:IREIAE>2.0.CO;2.

Paluch, I. R., and D. H. Lenschow (1991), Stratiform cloud formation in the marine boundary layer, *J. Atmos. Sci.*, *48*, 2141–2158, doi:10.1175/1520-0469(1991)048<2141:SCFITM>2.0.CO;2.

Penner, J. E., D. J. Bergmann, J. J. Walton, D. Kinnison, M. J. Prather, D. Rotman, C. Price, K. E. Pickering, and S. L. Baughcum (1998), An evaluation of upper troposphere NOx with two models, *J. Geophys. Res.*, *103*, 22,097–22,113, doi:10.1029/98JD01565.

Pruppacher, H. R., and J. D. Klett (1997), *Microphysics of Clouds and Precipitation*, 954 pp., Kluwer Acad., Norwell, Mass.

Ramaswamy, V., et al. (2001), Radiative forcing of climate change, in *Climate Change 2001: The Scientific Basis*, edited by J. T. Houghton et al., pp. 349–416, Cambridge Univ. Press, New York.

Rogers, R. R., and M. K. Yau (1989), *A Short Course in Cloud Physics*, 293 pp., Pergamon, New York.

Rotman, D. A., et al. (2004), IMPACT, the LLNL 3-D global atmospheric chemical transport model for the combined troposphere and stratosphere: Model description and analysis of ozone and other trace gases, *J. Geophys. Res.*, *109*, D04303, doi:10.1029/2002JD003155.

Saleeby, S. M., and W. R. Cotton (2004), A large-droplet mode and prognostic number concentration of cloud droplets in the Colorado State University regional atmospheric modeling system (RAMS). part I: Module description and supercell test simulations, *J. Appl. Meteorol.*, *43*, 182–195, doi:10.1175/1520-0450(2004)043<0182:ALMAPN>2.0.CO;2.

Shupe, M. D., and J. M. Intrieri (2004), Cloud radiative forcing of the Arctic surface: The influence of cloud properties, surface albedo, and solar zenith angle, *J. Clim.*, *17*, 616–628, doi:10.1175/1520-0442(2004)017<0616:CRFOTA>2.0.CO;2.

Simpson, J., and W.-K. Tao (1993), The Goddard Cumulus Ensemble model. part II: Applications for studying cloud precipitating processes and for NASA TRMM, *Terr. Atmos. Oceanic Sci.*, *4*, 73–116.

Smith, S. J., H. Pitcher, and T. M. L. Wigley (2001), Global and regional anthropogenic sulfur dioxide emissions, *Global Planet. Change*, *29*, 99–119, doi:10.1016/S0921-8181(00)00057-6.

Smith, S. J., R. Andres, E. Conception, and J. Lurz (2004), *Sulfur Dioxide Emissions: 1850–2000*, Pac. Northwest Natl. Lab., Richland, Wash.

Soong, S.-T., and Y. Ogura (1980), Response of trade wind cumuli to large-scale processes, *J. Atmos. Sci.*, *37*, 2035–2050, doi:10.1175/1520-0469(1980)037<2035:ROTCTL>2.0.CO;2.

Stevens, B., et al. (2003a), On entrainment rates in nocturnal marine stratocumulus, *Q. J. R. Meteorol. Soc.*, *129*, 3469–3492, doi:10.1256/qj.02.202.

Stevens, B., et al. (2003b), Dynamics and chemistry of marine stratocumulus-DYCOMS-II, *Bull. Am. Meteorol. Soc.*, *84*, 579–593, doi:10.1175/BAMS-84-5-579.

Tao, W.-K., and J. Simpson (1993), The Goddard Cumulus Ensemble model. part I: Model description, *Terr. Atmos. Oceanic Sci.*, *4*, 19–54.

Tao, W.-K., et al. (2003), Microphysics, radiation and surface processes in the Goddard Cumulus Ensemble (GCE) model, *Meteorol. Atmos. Phys.*, *82*, 97–137, doi:10.1007/s00703-001-0594-7.

Turner, D. D., et al. (2007), Thin liquid water clouds: Their importance and our challenge, *Bull. Am. Meteorol. Soc.*, *88*, 177–190, doi:10.1175/BAMS-88-2-177.

Twomey, S. (1974), Pollution and the planetary albedo, *Atmos. Environ.*, *8*, 1251–1256, doi:10.1016/0004-6981(74)90004-3.

Twomey, S. (1977), The influence of pollution on the shortwave albedo of clouds, *J. Atmos. Sci.*, *34*, 1149–1152, doi:10.1175/1520-0469(1977)034<1149:TIOPOT>2.0.CO;2.

Walko, R. L., W. R. Cotton, M. P. Meyers, and J. Y. Harrington (1995), New RAMS cloud microphysics parameterization: part I. The single-moment scheme, *Atmos. Res.*, *38*, 29–62, doi:10.1016/0169-8095(94)00087-T.

Wang, M., and J. E. Penner (2009), Aerosol indirect forcing in a global model with particle nucleation, *Atmos. Chem., Phys.*, *9*, 239–260.

Whitby, K. T. (1978), The physical characteristics of sulfur aerosols, *Atmos. Environ.*, *12*, 135–159, doi:10.1016/0004-6981(78)90196-8.

Xu, K.-M., et al. (2002), An intercomparison of cloud-resolving models with the Atmospheric Radiation Measurement summer 1997 intensive observation period data, *Q. J. R. Meteorol. Soc.*, *128*, 593–624, doi:10.1256/003590002321042117.

S. S. Lee and J. E. Penner, Department of Atmospheric, Oceanic, and Space Sciences, University of Michigan, 2455 Hayward Street, Room 1215, Ann Arbor, MI 48109, USA. (seoungl@umich.edu)

S. M. Saleeby, Department of Atmospheric Science, Colorado State University, Fort Collins, CO 80523, USA.